JACS
JOURNAL OF THE AMERICAN CHEMICAL SOCIETY
Article
pubs.acs.org/JACS

Ionic and Covalent Stabilization of Intermediates and Transition States in Catalysis by Solid Acids

Prashant Deshlahra, Robert T. Carr, and Enrique Iglesia*

Department of Chemical and Biomolecular Engineering, University of California, Berkeley, California 94720, United States

Supporting Information

ABSTRACT: Reactivity descriptors describe catalyst properties that determine the stability of kinetically relevant transition states and adsorbed intermediates. Theoretical descriptors, such as deprotonation energies (DPE), rigorously account for Brønsted acid strength for catalytic solids with known structure. Here, mechanistic interpretations of methanol dehydration turnover rates are used to assess how charge reorganization (covalency) and electrostatic interactions determine DPE and how such interactions are recovered when intermediates and transition states interact with the conjugate anion in W and Mo polyoxometalate (POM) clusters and gaseous mineral acids. Turnover rates are lower and kinetically relevant species are less stable on Mo than W POM clusters with similar acid strength, and such species are more stable on mineral acids than that predicted from W-POM DPE–reactivity trends, indicating that DPE and acid strength are essential but incomplete reactivity descriptors. Born–Haber thermochemical cycles indicate that these differences reflect more effective charge reorganization upon deprotonation of Mo than W POM clusters and the much weaker reorganization in mineral acids. Such covalency is disrupted upon deprotonation but cannot be recovered fully upon formation of ion pairs at transition states. Predictive descriptors of reactivity for general classes of acids thus require separate assessments of the covalent and ionic DPE components. Here, we describe methods to estimate electrostatic interactions, which, taken together with energies derived from density functional theory, give the covalent and ionic energy components of protons, intermediates, and transition states. In doing so, we provide a framework to predict the reactive properties of protons for chemical reactions mediated by ion-pair transition states.

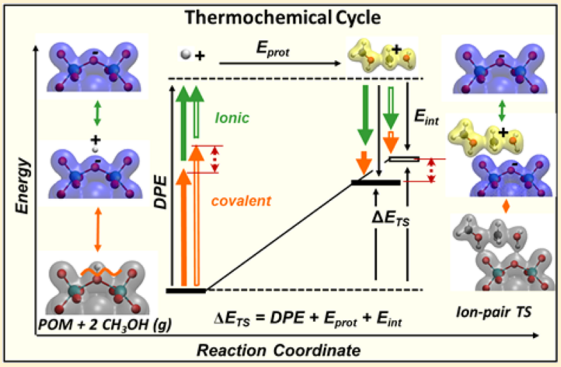

1. INTRODUCTION

Composition–function relations in catalysis seek to describe how the properties of solids influence reactivity by stabilizing the transition states (TS) and the reactive intermediates that ultimately define the activation barriers for the kinetically relevant elementary steps in catalytic sequences. For solids with known structures, such relations can be constructed on the basis of descriptors of reactivity accessible through theoretical estimates, which can then be used to assess the reactivity of hypothetical solids or to obtain measures of such descriptors for catalysts of uncertain structures.[1] Recent studies have established the effects of central atoms (X^{n+} = P^{5+}, Si^{4+}, Al^{3+}, Co^{2+}) in acid forms of W-based Keggin polyoxometalate clusters (W-POM; $H_{8-n}X^{n+}W_{12}O_{40})^{2-4}$ on deprotonation energies (DPE), a theoretical measure of acid strength, as well as the effects of DPE on rate constants for H_2O elimination from alkanol dehydration[5] and skeletal isomerization of alkenes via adsorbed alkoxides.[6,7]

DPE values define the energy required to remove a proton from an acid to noninteracting distances from the conjugate anion; thus, they represent probe-independent descriptors of acid strength, accessible through theoretical estimates for solids with known structures.[8,9] The reactivity of W-POM clusters with different central atoms correlates with their DPE because Brønsted acid catalysis proceeds by proton removal from the acid to form a cationic TS (e.g., methanol dehydration TS in Scheme 1), which becomes more stable when less energy is spent to deprotonate the stronger acids. Reactions differ in their dependence on acid strength because of the extent to which DPE effects are attenuated by interactions of the cationic TS with the conjugate anion.[6,10] The magnitude of this attenuation depends on the charge and the size of TS cations; small cations are more "proton-like" and interact more strongly with the POM anion, making their formation energy less sensitive to DPE.[6] The formation energies of reaction intermediates, which act as reference states for measured activation energies, may also depend on DPE because of the same factors that influence TS stability. Therefore, activation barriers become more sensitive to DPE when the energies of transition states are referenced to those of uncharged adsorbed species (E_a^{mono}, Scheme 1), which are insensitive to DPE because they do not require proton transfer, or of protons without interacting molecules than when reference intermediates are charged (E_a^{dimer}, Scheme 1) because, in the latter case, the

Received: July 3, 2014
Published: October 21, 2014

   dx.doi.org/10.1021/ja506149c | J. Am. Chem. Soc. 2014, 136, 15229–15247

Scheme 1. Energy Changes Due to Elementary Steps That Form Reactive Intermediates (CH_3OH Monomer and Dimer) and Transition State for DME Formation via Direct CH_3OH Dehydration Route on Brønsted Acids

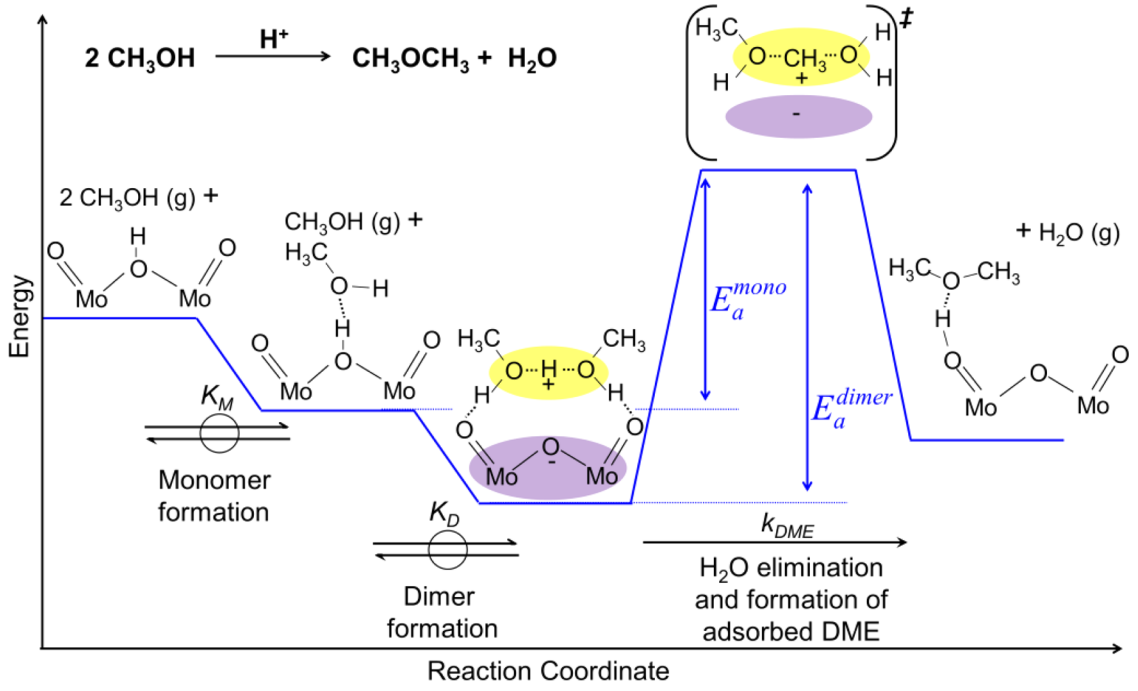

effects of DPE on the stability of transition states and reference states are similar and tend to cancel.[11]

Previous studies have developed rigorous relations between acid strength (DPE) and reactivity for solid acids of the W-POM type with different central atoms. Differences between their reactivity trends with DPE and those for another class of solid acids (zeolites) were interpreted in terms of additional stabilization of TS structures by solvation within the confined pore environments of microporous zeolite materials.[11,12] Mo-based POM clusters do not confine transition states or intermediates because of their mesoporous structures; yet, they exhibited much lower turnover rates for butanol dehydration than W-POM clusters for samples of equivalent DPE;[13] we surmised at the time that such differences arose from a weakening of the acid sites as a result of the possible reduction of the Mo-POM clusters by butanol reactants, which was qualitatively evident from observed changes in their color.[14] These studies did not show, however, whether, even in the absence of such extrinsic factors, turnover rates for a given reaction would become a single-valued function of acid strength for different classes of Brønsted acids.

Here, we contrast the reactivity and stability of reactive intermediates and transition states for methanol dehydration reactions on W-POM clusters with those on other classes of Brønsted acids (Mo-POM clusters, mineral acids in their gaseous form). These studies show that methanol dehydration proceeds via similar elementary steps on POM clusters with Mo and W addenda atoms and that changes in the central atom (S, P, Si, Al, Co) similarly influence the DPE and the reactivity in these two systems. Yet, measured first-order rate constants were much lower and adsorbed species were less stable on Mo-based than on W-based POM clusters of similar DPE values (and acid strength). In contrast, the adsorbed species were more stable and the predicted reactivities were higher on gaseous mineral acids than that on W-POM clusters with a similar DPE. We show here that such apparently disparate reactivities for catalysts with similar acid strengths reflect covalent and ionic contributions to DPE values, which are recovered to different extents in transition states, specifically because of the greater covalency of the H−Z bonds (Z^- is the conjugate anion) and the greater ionic character of ion-pair TS−Z structures. In this study, we develop and describe methods to calculate ionic and covalent components of interaction energies between cations and anions and also present a framework to incorporate them rigorously into descriptors of stability for reactive intermediates and transition states in general, using acid catalysis as a specific example.

2. METHODS

2.1. Catalyst Synthesis, Rates of CH_3OH−O_2 Reactions, and Titration of Acid Sites. Synthesis and characterization protocols and catalytic measurement methods have been described elsewhere in detail,[15] and only a brief description is provided here. $H_3PMo_{12}O_{40}$ (99.99%, Sigma-Aldrich) and $H_4SiMo_{12}O_{40}$ (99%, Aldrich) clusters were dispersed using incipient wetness impregnation of their aqueous solutions under ambient conditions on SiO_2 (Cab-O-Sil HS-5, 1.5 $cm^3\ g^{-1}$ pore volume) powders previously treated with 1 M HNO_3 and then in flowing dry air (UHP, Praxair, 0.83 $cm^3\ g^{-1}\ s^{-1}$) at 573 K for 5 h. Impregnated samples were stored in closed vials at ambient temperature for 24 h and then treated in flowing dry He (UHP, Praxair, 0.83 $cm^3\ g^{-1}\ s^{-1}$) at 323 K for 24 h. Samples were pressed, crushed, and sieved to retain 106−180 μm aggregates.

CH_3OH conversion rates and selectivities were measured on SiO_2-supported POM clusters (0.03−0.05 g; surface density 0.16 POM nm^{-2}) at 433 K using a tubular quartz flow reactor with plug-flow hydrodynamics. Samples were heated to reaction temperature (0.05 K s^{-1} heating rate) in 20% O_2 in He (99.999%, Praxair, 0.5 $cm^3\ s^{-1}$) and held for 0.5 h before rate measurements. Reactant mixtures contained CH_3OH (99.9%, Fisher Scientific), H_2O (doubly distilled and deionized), O_2 (99.999%, Praxair), and He (99.999%, Praxair). CH_3OH and H_2O were introduced as liquids into a flowing O_2/He stream at 393 K; liquid and gas flow rates were controlled to set the desired CH_3OH, H_2O, and O_2 pressures (0.15−4, 2.7, and 20 kPa, respectively) and the residence times required to maintain <20% CH_3OH conversions.

Reactant and product concentrations were measured by gas chromatography (Agilent 6890) using a methyl silicone capillary column connected to a flame ionization detector and a Porapak Q packed

dx.doi.org/10.1021/ja506149c | J. Am. Chem. Soc. 2014, 136, 15229−15247

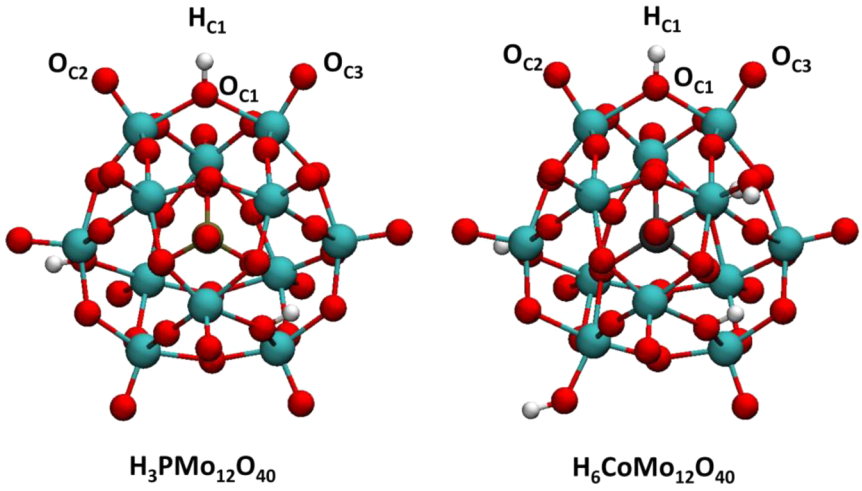

Figure 1. Optimized structures of $H_3PMo_{12}O_{40}$ and $H_6CoMo_{12}O_{40}$ clusters. Protons (H_{C1}) and local O atoms that constitute the active sites in DFT calculations are indicated.

column connected to a thermal conductivity detector. Dimethyl ether (DME), formaldehyde (HCHO), methyl formate (MF), dimethoxymethane (DMM), and H_2O were the only products detected. Rates are reported as molar formation rates of DME and of oxidative dehydrogenation (ODH) products. DME formation rates (r_{DME}) are normalized by the number of accessible protons, measured by titration with 2,6-di-*tert*-butylpyridine (DTBP) during CH_3OH-O_2 reactions (4 kPa CH_3OH, 2.7 kPa H_2O, 20 kPa O_2, 7 Pa DTBP). ODH rates are defined as the sum of HCHO, MF, and DMM molar formation rates because these products all require initial oxidation of one CH_3OH to HCHO (Supporting Information, Scheme S1). Kinetic constants were determined by regressing rate data to integral form of rate equations.

2.2. Computational Methods. Structures and energies of stable intermediates, transition states, gaseous reactants and products, and charged cations and anions were calculated using periodic gradient-corrected density functional theory (DFT) as implemented in the Vienna ab initio simulation package (VASP).[16] Wavefunctions for valence electrons were represented using a periodic plane-wave basis-set expansion to a cutoff energy of 396.0 eV. Vanderbilt ultrasoft pseudopotentials (USPP)[17] were used to describe electron–core interactions. Exchange and correlation energies were calculated within the generalized-gradient approximation using the Perdew–Wang (PW91) functional.[18] Electronic structures were calculated by specifying integer band occupancies and were converged self-consistently to energies $<1 \times 10^{-6}$ eV for each step in both structural optimizations and single-point calculations. Calculation of Keggin clusters with Co central atoms were performed with spin-polarization and three unpaired electrons, corresponding to the Co^{2+} electronic configuration. Spin-restricted calculations were used for all other compositions.

Full Keggin clusters (1.1 nm diameter) and the smaller structures of mineral acids and of gaseous molecules were calculated at the center of a $2 \times 2 \times 2$ nm^3 unit cell to provide a sufficient vacuum region that prevents interactions among clusters in adjacent unit cells. A $1 \times 1 \times 1$ Monkhorst–Pack k-point mesh was used to sample the first Brillouin zone. Structures of all stable intermediates were optimized until forces on all atoms were <0.05 eV Å^{-1}. Calculations of charged species, such as protons and conjugate cluster anions required for DPE estimates and ion-pair interaction energies, were performed with uniform background charges to maintain neutral unit cells and correction to energies using methods[19] implemented in VASP. Dipole and quadrupole moments were calculated with the center of the unit cell taken as the center of charge and were used to correct for long-range interactions between neighboring unit cells in both charged and neutral systems. Structures of transition states were determined using the nudged elastic band (NEB)[20] and dimer[21] methods, as reported elsewhere.[11] The electronic and geometric steps in NEB calculations were converged to energies $<1 \times 10^{-4}$ eV and forces on atoms, <0.3 eV Å^{-1}; respective convergence criteria for dimer calculations were 1×10^{-7} eV and 0.05 eV Å^{-1}. Calculated energies were not corrected for zero-point vibrational energies (ZPVE) because such corrections are expected to be similar in magnitude for species of a given type and molecular composition adsorbed on different POM compositions.

The stabilities of reactive intermediates and transition states for CH_3OH reactions were calculated using energies of structurally relaxed surface species at a particular proton on POM clusters shown in Figure 1 (H_{C1}), of bare clusters, and of gaseous molecules. Deprotonation energies (DPE) for POM clusters and other acids are defined as the energy required to remove a proton from an acid (HA) to form an isolated proton (H^+) and a structurally relaxed isolated anion (A^-)

$$\mathrm{DPE} = E^{H^+} + E^{A^-} - E^{HA} \quad (1)$$

Interaction energies of organic cations with POM anions were calculated using energies of fully relaxed isolated cations and anions; these energies are required in the thermochemical cycles relating stability of surface species to the DPE of POM clusters.

The reliability of the results obtained from the DFT treatments described above and used in this work was tested by varying the edge length of the cubic unit cell between 1.5 and 3 nm, by changing the treatment of atom cores from USPP to projector augmented wave (PAW) method,[22] and by performing molecular DFT calculations with localized basis sets using the Gaussian program[23] (Supporting Information, Section S11). These variations have only small effects on DPE values for POM clusters and gaseous mineral acids (Supporting Information, Section S11), which cannot change any conclusions regarding the effect of compositions or cause a significant shift in the numerical values of the results.

Electrostatic interaction energies (E_{es}) for ion pairs can be derived from classical calculations because Hellman–Feynmann theorem states that once the electron distribution has been determined from quantum mechanics, all forces on molecules,[24] and by extension the interaction energies,[25] can be rigorously calculated by considering only the classical effects. E_{es} values were calculated by numerical integration[26,27] of the Coulomb interactions between DFT-derived charge density distributions of structurally relaxed cations and anions; such distributions are expressed as a three-dimensional mesh spanning the calculation unit cell, and each element of the mesh is denoted as a mesh cell. The calculated E_{es} is the sum of repulsion between atom cores (i.e., nucleus and inner electrons treated as a point charge at the center) and valence electrons and of attraction between atom cores and electrons of the cation and anion species

dx.doi.org/10.1021/ja506149c | J. Am. Chem. Soc. 2014, 136, 15229–15247

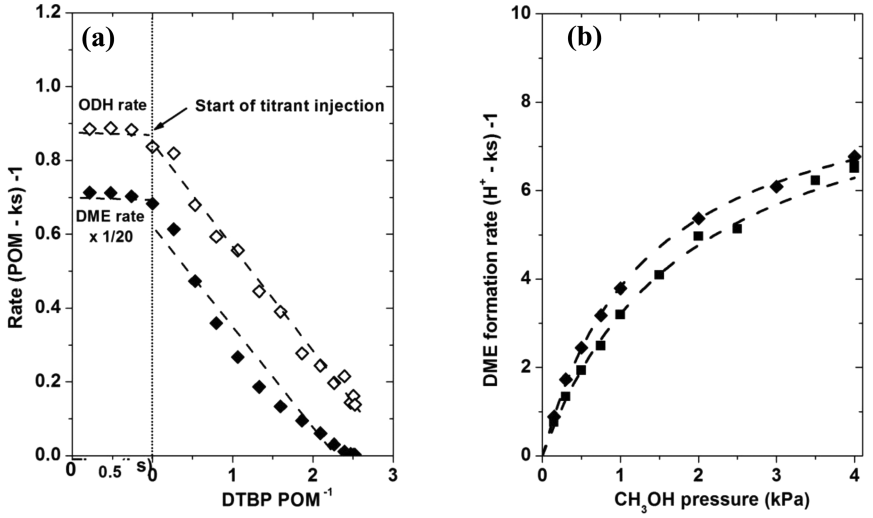

Figure 2. (a) DME formation (filled diamonds) and ODH (open diamonds) rates per POM for CH_3OH-O_2 reactions on $H_3PMo_{12}O_{40}/SiO_2$ as a function of time before DTBP injection (433 K, 4 kPa CH_3OH, 20 kPa O_2, 2.7 kPa H_2O) and of cumulative titrant uptake after DTBP injection (7 Pa DTBP). (b) DME turnover rates (per accessible proton) as a function of CH_3OH pressure on H_3PMo/SiO_2 (filled diamonds) and H_4SiMo/SiO_2 (filled squares) (surface density 0.16 POM nm^{-2}; 433 K, 20 kPa O_2, 2.7 kPa H_2O). Dashed curves reflect best regression fits to the form of eq 5.

$$E_{es} = \frac{1}{4\pi\varepsilon_0}\left[\sum_{c=1}^{N}\sum_{a=1}^{M}\frac{Z_a Z_c}{r_{ac}} + \sum_{c=1}^{T}\sum_{a=1}^{S}\frac{(\rho_a\Delta V)(\rho_c\Delta V)}{r_{ac}} + \sum_{c=1}^{T}\sum_{a=1}^{M}\frac{Z_a(\rho_c\Delta V)}{r_{ac}} + \sum_{a=1}^{S}\sum_{c=1}^{N}\frac{Z_c(\rho_a\Delta V)}{r_{ac}}\right] \quad (2)$$

where ε_0 is the permittivity of free space, Z_a and Z_c are charges of atom cores of the anion and cation respectively, ρ_a and ρ_c are electronic charge densities of anion and cation at a given mesh cell, respectively, ΔV is the volume of a mesh cell, r_{ac} are separations between the atom cores and mesh cells in anion and cation distributions, M and N are total numbers of atom cores in the anion and the cation, respectively, and S and T are total number of mesh cells in the anion and the cation, respectively. Charge distributions were calculated on a 210 × 210 × 210 mesh spanning a 2 nm cubic unit cell (yielding 0.0095 nm cubic mesh cells); meshes of higher and lower resolution (280 and 140 cubic mesh, respectively) did not affect the calculated energies (Supporting Information, Section S2.2). E_{es} calculations from eq 2 required partitioning of the unit cell volume into cation and anion regions[27] to avoid terms with $r_{ac} = 0$ (except when the cation is just a point charge, as in the case of a proton); it was achieved by adding charge distributions of isolated cations and anions, followed by partitioning using the Bader method,[28,29] which divides the charge density across planes of zero flux. An illustration of the unit cell partitioning and comparisons of interaction energies between simple spherical charge distributions (interactions of H^+ with F^{1-}, Cl^{1-}, Br^{1-}, and I^{1-} and of H^0 with H^0) derived from numerical integrations (eq 2) with values calculated using their analytical expression (Supporting Information, eq S.1), which confirm the accuracy of such integrations, are shown in the Supporting Information (Section S2).

The Bader method[28,29] was used to calculate charges on reaction intermediates and transition states and to explore electronic effects of deprotonating the POM clusters by calculating charges on their central tetrahedra and oxide shells. The spatial relaxation of the anion charge upon deprotonation was also estimated by calculating the displacement of the center of the charge distribution between the relaxed and unrelaxed anions. The center of charge at the anion ($\langle\vec{r}_a\rangle$) was calculated by taking a ratio of the first and zeroth moments of the DFT-derived charge distributions[30]

$$\langle\vec{r}_a\rangle = \frac{\sum_{a=1}^{M}\vec{r}_a Z_a + \sum_{a=1}^{S}\vec{r}_a\rho_a\Delta V}{\sum_{a=1}^{M}Z_a + \sum_{a=1}^{S}\rho_a\Delta V} \quad (3)$$

Here, $\vec{r}_a$ represents x, y, and z coordinates of the center of an atom core (nucleus and core electrons) or a mesh cell (an element of the charge density distribution mesh) in the charge distribution of a POM anion, whereas the other symbols are defined as in eq 2.

3. RESULTS AND DISCUSSION

3.1. CH_3OH Dehydration Turnover Rates and Reaction Pathways from Experiment and Theory. The number of Brønsted acid sites responsible for CH_3OH dehydration catalysis was determined by titration of protons with di-*tert*-butylpyridine (DTBP) during catalytic reactions (Figure 2a). DTBP molecules are selective titrants of Brønsted acid sites because steric constraints prevent their coordination to Lewis acid centers.[31] Saturation uptakes of DTBP fully suppressed dehydration rates, indicating that all accessible protons were titrated and that any Lewis acid sites present did not catalyze dehydration at detectable rates. These Brønsted acid site counts, determined from saturation uptakes of DTBP, are used here to normalize CH_3OH dehydration rates on silica-supported Mo-POM clusters as turnover rates in order to rigorously compare the reactivity of protons among catalysts with different composition (and acid strength). The number of protons accessible to DTBP was smaller than values expected for stoichiometric $H_3PMo_{12}O_{40}$ and $H_4SiMo_{12}O_{40}$ clusters (by factors of 0.8 and 0.6, respectively; Table 1). The "missing" protons may reflect the formation of water via condensation with other POM clusters to form secondary structures or with silanols to form siloxane bridges.[32]

Table 1. Number Protons per POM Cluster Titrated by DTBP during CH_3OH-O_2 Reactions[a] and First-Order (k_{mono}) and Zero-Order (k_{dimer}) DME Formation Rate Constants on $H_3PMo_{12}O_{40}/SiO_2$ and $H_4SiMo_{12}O_{40}/SiO_2$[b,c]

composition	accessible H^+ (per POM cluster)	k_{mono} (molecules $H^{+\,-1}$ kPa^{-1} ks^{-1})	k_{dimer}
H_3PMo/SiO_2	2.5	6.6 (±0.3)	9.3 (±0.4)
H_4SiMo/SiO_2	2.2	4.9 (±0.6)	8.9 (±1.0)

[a]At 4 kPa CH_3OH, 2.7 kPa H_2O. [b]Surface density 0.16 POM nm^{-2}; 20 kPa O_2, 433 K. [c]Reported uncertainties reflect 95% confidence intervals.

dx.doi.org/10.1021/ja506149c | J. Am. Chem. Soc. 2014, 136, 15229−15247

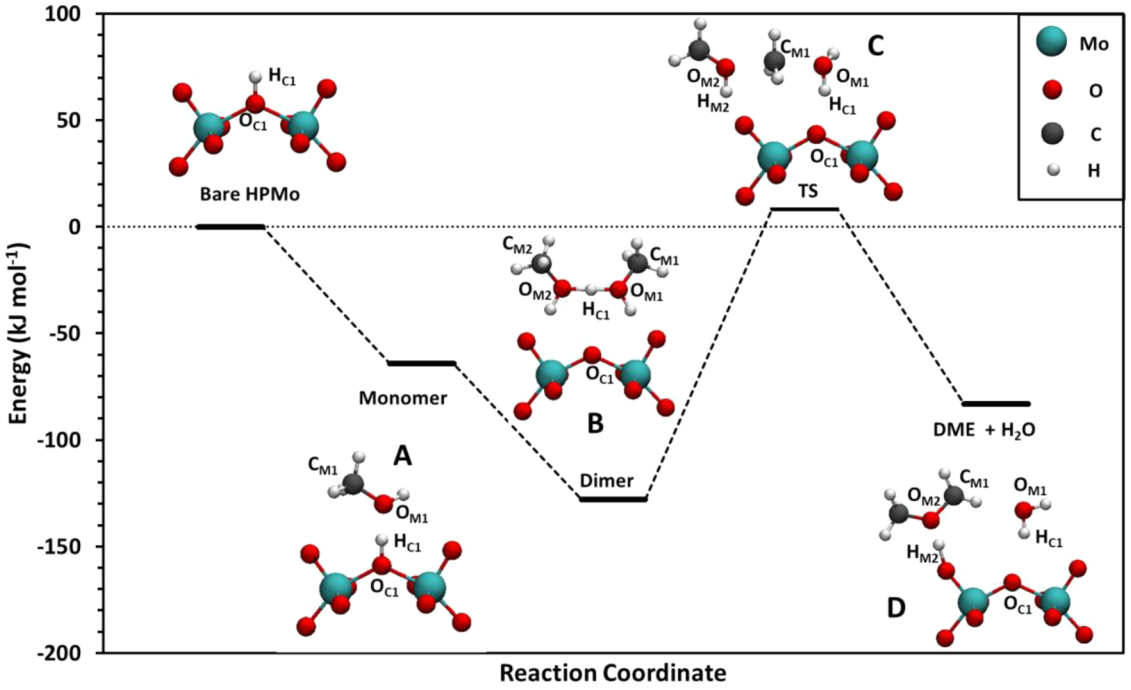

Figure 3. Calculated structures and energies of reactive intermediates and transition state for direct dehydration route in which H-bonded CH_3OH reacts with another CH_3OH to form DME on a $H_3PMo_{12}O_{40}$ cluster.

Figure 2b shows CH_3OH dehydration turnover rates on $H_3PMo_{12}O_{40}$ and $H_4SiMo_{12}O_{40}$ as a function of CH_3OH pressure (0.15−4.0 kPa). Turnover rates increased linearly with CH_3OH pressure at low pressure values on both catalysts, but the rate dependence became less sensitive to pressure as pressure increased. Such shifts from first-order to zero-order kinetic dependences are reminiscent of Langmuir-type rate equations, previously reported to describe dehydration rate data on W-POM clusters with different central atoms[11]

$$\frac{r_{DME}}{[H^+]} = \frac{\alpha P_{CH_3OH}}{1 + \beta P_{CH_3OH}} \quad (4)$$

The chemical origins of the α and β parameters have been mechanistically interpreted[3] on the basis of two plausible sequences of elementary steps, both of which can account for the functional form of eq 4. One possible route involves the sequential elimination of H_2O from bound CH_3OH monomers to form methoxide species, which then react with a gaseous CH_3OH molecule to form DME. An alternate route involves direct H_2O elimination from protonated CH_3OH dimers that form via reactions of gaseous CH_3OH with H-bonded CH_3OH monomers. Our DFT estimates of the energies of transition states for these two routes on both W-POM and Mo-POM (Supporting Information, Figure S5), and previous estimates on W-POM clusters[11] show that the latter route prevails on both W and Mo POM clusters (Supporting Information, Figure S5). As a result, only the direct dehydration pathway is considered in the discussion that follows.

Scheme 1 shows the elementary steps that mediate direct dehydration routes. Quasi-equilibrated adsorption of a CH_3OH molecule, the product of which we denote as the monomer intermediate, is followed by quasi-equilibrated adsorption of a second CH_3OH molecule to form a dimer, onto which the proton is transferred to form cationic intermediates. These dimers rotate to form coadsorbed charged structures with the atomic orientation required to eliminate water and form DME in a step mediated by the transition state for this elimination reaction. Turnovers are completed by desorption of the DME molecules formed in the elimination step. These steps and reversibility assumptions, taken together with the formalism of the pseudo-steady-state hypothesis for all surface intermediates, give a rate equation (derivation in Supporting Information, Section S4) that follows a Langmuirian form

$$\frac{r_{DME}}{[H^+]} = \frac{k_{mono} P_{CH_3OH}}{1 + \frac{k_{mono}}{k_{dimer}} P_{CH_3OH}} \quad (5)$$

Here, the first-order rate constant k_{mono} (= $k_{DME}K_D$ in terms of rate and equilibrium constants shown in Scheme 1) and the zero-order rate constant k_{dimer} (= k_{DME}) represent the apparent rate constants for CH_3OH dehydration under conditions that lead to monomer and protonated dimers, respectively, at saturation coverages on all accessible Brønsted acid sites. Dashed lines in Figure 2b represent the regression of rate data to the functional form of eq 5.

DME formation transition states (TS) and the reactive intermediates (monomer and protonated dimer) that act as reference species for measured rate constants (k_{mono} and k_{dimer}, respectively) were previously proposed on the basis of DFT calculations on W-POM clusters.[11] Figure 3 shows the optimized structures and energies of formation of these species on $H_3PMo_{12}O_{40}$ clusters (bond distances and Bader charges in Supporting Information, Table S2). The formation energy of the TS (ΔE^{TS}) was calculated using DFT-derived energies of the TS (E^{TS}), the bare cluster (E^{HA}), and gaseous CH_3OH molecules ($E^{CH_3OH(g)}$)

$$\Delta E^{TS} = E^{TS} - E^{HA} - 2E^{CH_3OH(g)} \quad (6)$$

The formation energies of monomer (ΔE^{mono}) and dimer (ΔE^{dimer}) species were calculated using the analog of eq 6 and their respective DFT-derived energies (E^{mono} and E^{dimer}).

dx.doi.org/10.1021/ja506149c | J. Am. Chem. Soc. 2014, 136, 15229−15247

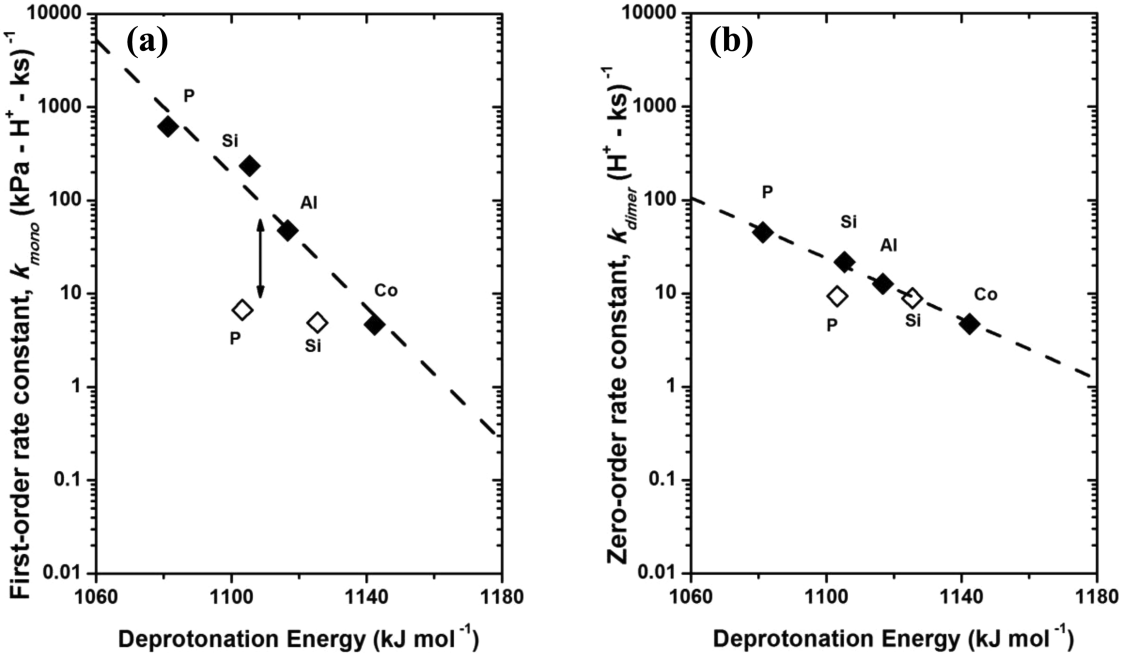

Figure 4. Measured (a) first-order (k_{mono}, eq 5) and (b) zero-order (k_{dimer}, eq 5) rate constants for DME formation (433 K) on $H_{8-n}X^{n+}Mo_{12}O_{40}/SiO_2$ (X^{n+} = P^{5+}, Si^{4+}) and those previously measured on $H_{8-n}X^{n+}W_{12}O_{40}/SiO_2$ (X^{n+} = P^{5+}, Si^{4+}, Al^{3+}, Co^{2+})[11] as a function of calculated DPE. DPE of bare POM clusters are used even though the clusters are covered with H-bonded CH_3OH and dimers under conditions that lead to k_{mono} and k_{dimer}, respectively. Saturation coverages increase the DPE of clusters, but by similar extents for W and Mo POM clusters and therefore do not significantly affect the relative magnitudes of rate constants (Supporting Information, Table S3 and Figure S6).

Monomers (Figure 3, structure A) adsorb onto protons (H_{C1}) via strong H-bonding, which elongates the O−H bond in the POM cluster (O_{C1}−H_{C1}) from 0.097 to 0.105 nm. This O_{C1}−H_{C1} distance, however, remains much shorter than that between the proton and the O atom in CH_3OH (H_{C1}−O_{M1}, 0.145 nm), suggesting that CH_3OH monomers are not protonated, a conclusion consistent with their very small Bader charges (+0.10 e). The protonated dimer, formed via the reaction of a second CH_3OH with the monomer, causes the proton to separate from the cluster and to reside between the O atoms of the two CH_3OH molecules in the dimer structure (Figure 3, structure B). The $(CH_3OH)_2H^+$ structure thus formed is charged (+0.87 e Bader charge) and interacts with the conjugate POM anion. The dimer rearranges to orient the C atom of one CH_3OH molecule toward the O atom of the other molecule in order to form the DME formation TS (Figure 3, structure C); this TS structure resembles a CH_3^+ carbenium ion stabilized by ion-dipole interactions with the O atoms in the H_2O and the CH_3OH molecules and through ion-pair interactions with the POM conjugate anion. The CH_3OH−CH_3^+−H_2O TS structure is charged (+0.90 e Bader charge), consistent with the ubiquitous involvement of ion-pair transition states in mediating acid-catalyzed reactions.[10,33] The two measured rate constants (k_{mono} and k_{dimer}), therefore, reflect the stability of a charged TS with respect to a neutral monomer (k_{mono}) and a charged dimer (k_{dimer}) species.

These measurements and calculations show that the dehydration kinetics previously established for W-POM are also consistent with Mo-POM rate data and DFT estimates; therefore, mechanistic differences cannot account for any differences observed in the turnover rates of the two classes of POM clusters at equivalent acid strengths. Next, we compare the values of measured rate constants and the calculated energies of all kinetically relevant surface species for these two classes of solid acids.

3.2. Effect of Brønsted Acid Composition on Rate Constants and Stability of Surface Species. CH_3OH dehydration to DME and CH_3OH oxidative dehydrogenation (ODH) reactions occur concurrently on Mo-POM because MoO_x addenda species can undergo redox cycles and catalyze oxidation reactions using lattice O atoms, which are then replenished by O_2 during each catalytic ODH turnover.[34] ODH reactions can plausibly corrupt the measurement of DME formation kinetics by introducing competing or inhibiting surface intermediates or by changing the structure or the valence of POM clusters as lattice oxygens react during these redox cycles. Therefore, the effect of such factors on DME formation turnover rates on bifunctional Mo-POM clusters must be assessed for comparing them with the corresponding rates on monofunctional and nonreducible W-based POM clusters.

Mechanistic interpretations of CH_3OH−O_2 reaction rates on Mo-POM[15] have shown that ODH rates decrease upon addition of H_2O to CH_3OH−O_2 reactants because H_2O and reactive CH_3OH species adsorb competitively at redox sites. DME formation rates, however, are not affected by H_2O, suggesting that acid catalysis occurs at sites distinct from redox sites, on which H_2O does not significantly adsorb.[15] These conclusions are consistent with DFT estimates of H-addition energies (HAE; a descriptor of the stability of the rate-limiting H-abstraction TS for ODH), which suggest that the HAE values of the O atoms bound to the proton (acid sites) in POM clusters are much less negative than those for O atoms away from protons; the latter O atoms, therefore, act as the active redox sites in ODH catalysis.[15]

ODH reactions reduce Mo centers in POM clusters via hydrogenation of lattice O atoms as part of the catalytic redox cycle. These reduced centers lead to higher DPE values for POM protons;[32] thus, DPE values depend on the extent of reduction during ODH catalysis, which is set by the kinetic coupling between kinetically relevant reduction steps and the reoxidation

dx.doi.org/10.1021/ja506149c | J. Am. Chem. Soc. 2014, 136, 15229−15247

of the reduced centers by O_2 (and thus by the CH_3OH/O_2 ratio in reactants). Measured ODH rates did not depend on O_2 pressure, suggesting that reoxidation steps are fast and that the number of reduced centers remains very small during steady-state ODH catalysis.[15] The extent of reduction is particularly low at high O_2 pressure and in the presence of H_2O (20 kPa O_2; 2.7 kPa H_2O), as shown by in situ UV−visible spectroscopy.[14,15] Under these conditions, DME formation turnover rates reflect the CH_3OH dehydration reactivity of fully oxidized Mo-POM clusters; such rates are compared here with previously measured rates on W-POM clusters,[11] which remain fully oxidized during CH_3OH dehydration catalysis, even in the absence of O_2.

First-order (k_{mono}) and zero-order (k_{dimer}) rate constants were determined by regressing measured CH_3OH dehydration rates to the functional form of eq 5. Both rate constants decreased exponentially with increasing DPE values on W-POM clusters with different central atoms (Figure 4),[11] consistent with activation energies (E_a) that increased proportionally with increasing DPE values

$$\frac{dE_a}{dDPE} = -RT\frac{d\ln k}{dDPE} \quad (7)$$

The larger slope of k_{mono} relative to that of k_{dimer} in these plots (Figure 4) reflects activation energies that depend more sensitively on DPE when the DME formation TS energies are referenced to neutral monomers (slope of $-RT \ln k_{mono}$ versus DPE plot 0.30 ± 0.12; Figure 4a and Table 2) than when referenced to protonated dimers (slope of $-RT \ln k_{dimer}$ versus DPE plot 0.13 ± 0.09; Figure 4b and Table 2). For an equivalent DPE value, Mo-POM clusters show lower k_{mono} values than W-POM clusters (Figure 4a; k_{mono} values on $H_3PMo_{12}O_{40}$ and $H_4SiMo_{12}O_{40}$ are 22 and 5 times lower, respectively, than the W-POM trend line, reflecting 11 and 6 kJ mol^{-1} higher respective activation energies calculated from differences in $-RT \ln k_{mono}$ values at 433 K; eq 7). In contrast, k_{dimer} values are similar on Mo-POM and W-POM clusters (Figure 4b; activation energy differences <2 kJ mol^{-1}, calculated from differences in $-RT \ln k_{dimer}$ values at 433 K; eq 7), suggesting that Mo-POM clusters show lower reactivity than W-POM when activation barriers are referenced to neutral monomers (k_{mono}) but not when referenced to charged dimers (k_{dimer}).

Table 2. Dependences of Calculated Formation Energies of Monomers (ΔE^{mono}), Protonated Dimers (ΔE^{dimer}), and DME Formation Transition States (ΔE^{TS}); Activation Energies (E_a^{mono} and E_a^{dimer}); Measured Rate Constants on the DPE Changes within a Given Class of Brønsted Acids; and Offsets of These Values on Mo-POM and Mineral Acids from Those on W-POM as Shown in Figures 5 and 6[a]

		offset (difference between intercepts) (kJ mol^{-1})	
quantity	linear dependence on DPE (slope)	$\Delta E_{Mo\text{-}POM} - \Delta E_{W\text{-}POM}$	$\Delta E_{mineral\ acids} - \Delta E_{W\text{-}POM}$
ΔE^{mono} [b]	0.15 (±0.04)	5 (±2)	−18 (±4)
ΔE^{dimer} [b]	0.38 (±0.08)	14 (±4)	
ΔE^{TS} [b]	0.29 (±0.06)	15 (±3)	−39 (±4)
E_a^{mono} [c]	0.14 (±0.05)	10 (±2)	−21 (±8)
E_a^{dimer} [c]	−0.09 (±0.05)	1 (±3)	
$-RT \ln k_{mono}$ [d]	0.30 (±0.12)		
$-RT \ln k_{dimer}$ [d]	0.13 (±0.09)		

[a]Reported uncertainties reflect 95% confidence intervals. [b]Derived from eq 6 and its analogs for monomers and dimers (values in Figure 5). [c]Derived from eqs 8 and 9 (values in Figure 6). [d]Measured rate constants regressed to the functional form of eq 7, 433 K.

These smaller k_{mono} values on Mo-POM than on W-POM at equivalent DPE values may reflect (i) structural or electronic changes induced by even slight reduction during concurrent ODH reactions on Mo-POM[15] (in spite of conditions that minimize such effects) or (ii) a lower intrinsic stability of TS relative to monomers on Mo-POM than on W-POM because effects of acid strength manifest themselves differently in these two catalytic systems (in spite of their identical catalytic sequences and kinetically relevant steps). DFT methods can determine any contributions from the latter effects by comparing stabilities of relevant surface species and transition states on fully oxidized Keggin forms of W and Mo clusters; such calculations specifically remove any effects of reaction-induced changes in POM structure or oxidation state.

Figure 5 shows the formation energies of monomers (ΔE^{mono}), dimers (ΔE^{dimer}), and DME formation transition states (ΔE^{TS}; eq 6) on Mo and W POM clusters and of monomers (ΔE^{mono}) and transition states (ΔE^{TS}) on gaseous mineral acids, as a function of the DPE of these Brønsted acids. Structures of monomers and transition states were similar on all acids, whereas dimer species were protonated on all POM clusters but not on mineral acids (Supporting Information; bond lengths and structures in Tables S2 and S4, respectively). Therefore, the energies of dimers on mineral acids are not compared here with those on POM clusters. Within a given type of acid (W-POM, Mo-POM, mineral acids), all surface species became less stable with increasing DPE on acids with different central atoms, resulting in a linear increase in ΔE with DPE (Figure 5); their slopes were identical on Mo and W POM within statistical uncertainty ($d\Delta E/dDPE$ values in Table 2). The stability of neutral monomers was less sensitive to DPE ($d\Delta E^{mono}/dDPE$ = 0.15 ± 0.04; Figure 5a and Table 2) than for protonated dimers ($d\Delta E^{dimer}/dDPE$ = 0.38 ± 0.08; Figure 5a and Table 2) or TS ion pairs ($d\Delta E^{TS}/dDPE$ = 0.29 ± 0.06; Figure 5b and Table 2), as also found previously for W-POM clusters.[11]

Activation energies (E_a^{mono} and E_a^{dimer}) for first-order (k_{mono}) and zero-order (k_{dimer}) rate constants reflect the stability of the DME formation TS referenced to neutral monomers and protonated dimers, respectively

$$E_a^{mono} = \Delta E^{TS} - \Delta E^{mono} \quad (8)$$

$$E_a^{dim\ er} = \Delta E^{TS} - \Delta E^{dimer} \quad (9)$$

E_a^{mono} values were more sensitive to DPE than E_a^{dimer} ($dE_a^{mono}/dDPE$ = 0.14 ± 0.05, $dE_a^{dimer}/dDPE$ = −0.09 ± 0.05; Figure 6 and Table 2); these findings are consistent with measured k_{mono} values that are more sensitive to DPE than k_{dimer} values (slopes 0.30 ± 0.12 and 0.13 ± 0.09, respectively; Figure 4 and Table 2). The measured effects of DPE on rate constants were stronger than those given by calculations because the DPE values used are for bare clusters (Figure 4) but monomers and dimers saturate the acid sites under conditions that reflect k_{mono} and k_{dimer}, respectively. Proton−CH_3OH interactions in saturated clusters increase DPE values for vicinal protons (Supporting Information, Table S3; $DPE_{dimer,sat} > DPE_{mono,sat} > DPE_{bare}$), and larger DPE values (on bare clusters with different central atoms) increase more strongly upon cluster saturation with monomers and dimers ($dDPE_{sat}/dDPE_{bare} > 1$; Supporting Information, Table S3). As a result, the dependence of measured rate constants on DPE_{sat} is weaker than that on DPE_{bare} ($-RT\ d\ln k_{mono}/dDPE_{mono,sat} < -RT$

dx.doi.org/10.1021/ja506149c | J. Am. Chem. Soc. 2014, 136, 15229−15247

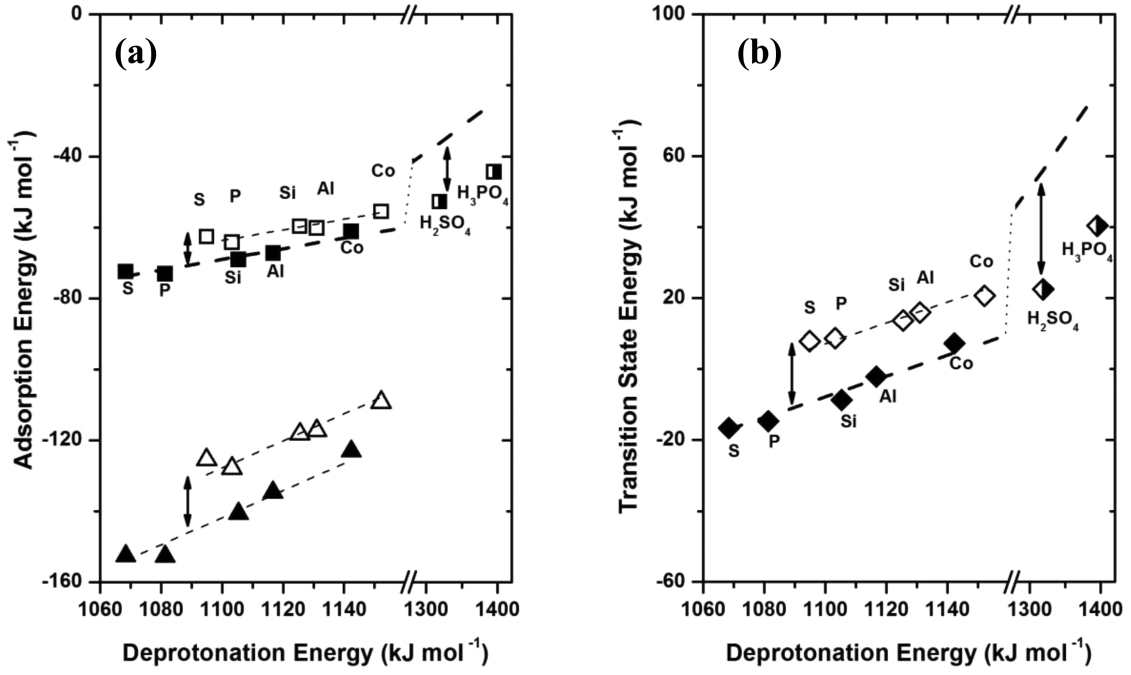

Figure 5. Calculated adsorption energies of (a) monomers (closed squares, open squares, half-open squares) and protonated dimers (closed triangles, open triangles) and (b) DME formation TS (closed diamonds, open diamonds, half-open diamonds) on $H_{8-n}X^{n+}W_{12}O_{40}$ (closed symbols) and $H_{8-n}X^{n+}Mo_{12}O_{40}$ (open symbols) POM clusters and $H_{8-n}X^{n+}{}_2O_4$ gaseous mineral acids (half-open symbols) as a function of their DPE ($X^{n+} = S^{6+}$, P^{5+}, Si^{4+}, Al^{3+}, Co^{2+}). Protonated dimers were not stable on mineral acids. Dashed lines reflect best linear regression fits with identical slopes assumed for W-POM and Mo-POM clusters. W-POM trend lines are extrapolated to compare with mineral acids at their DPE values. Vertical arrows reflect offsets between energies on W-POM and those on other compositions.

d ln k_{mono}/dDPE$_{bare}$; $-RT$ d ln k_{dimer}/dDPE$_{dimer,sat}$ < $-RT$ d ln k_{dimer}/dDPE$_{bare}$) and closer to calculated dE_a/dDPE values (Supporting Information; Figure S6). Such coverage effects are similar on Mo and W POM clusters (Supporting Information, Table S3); therefore, coverage effects do not affect the relative values of these rate constants on Mo and W POM clusters with equivalent DPE$_{bare}$ (Figure 4). They also do not affect theoretical comparisons among these POM clusters (Figures 5 and 6) because theoretical treatments were restricted to bare clusters.

DFT-derived stabilities of monomers, dimers, and TS species and activation energies are not single-valued functions of DPE values among the different classes of Brønsted acids (even though each one depends linearly on DPE as the central atom is changed), as shown by the offsets between W and Mo POM clusters and mineral acids in Figures 5 and 6. For a given DPE value (and acid strength), all surface species are less stable on Mo than on W POM and more stable on mineral acids than on POM clusters (Figure 5 and Table 2). Activation energies referenced to monomers are higher on Mo-POM and lower on mineral acids than on W-POM clusters ($E^{mono}_{a,Mo\text{-}POM} - E^{mono}_{a,W\text{-}POM}$ = 10 kJ mol^{-1}; $E^{mono}_{a,mineral\ acid} - E^{mono}_{a,W\text{-}POM}$ = −21 kJ mol^{-1}; Figure 6 and Table 2) for the same DPE value; in contrast, those referenced to dimers are similar for Mo and W POM ($E^{dimer}_{a,Mo\text{-}POM} - E^{dimer}_{a,W\text{-}POM}$ = 1 kJ mol^{-1}; Figure 6 and Table 2), consistent with the smaller k_{mono} values measured on Mo than on W POM clusters, but the similar k_{dimer} values measured on both Mo and W POM clusters (Figure 4). The offsets in E^{mono}_a for Mo and W POM clusters (10 kJ mol^{-1}) were calculated on fully oxidized clusters; thus, they are not affected by any reaction-induced catalyst changes. Yet, these offsets are similar to those found for k_{mono} values (Figure 4 and eq 7; E_a = 11 and 6 kJ mol^{-1} higher on $H_3PMo_{12}O_{40}$ and $H_4SiMo_{12}O_{40}$, respectively, than that on W-POM), suggesting that intrinsic differences exist in TS stabilization for the same value of DPE on W and Mo POM clusters. Such effects may account, at least in part, for the difference in measured reactivity at equivalent acid strengths.

The effects of DPE (for W-POM clusters with different central atoms) on TS stabilities (dΔE^{TS}/dDPE < 1; Table 2) were interpreted previously[11] using thermochemical cycles that describe the energy of surface species via those involved in the hypothetical path[35] depicted in Scheme 2. These cycles allow TS formation energies (ΔE^{TS}) to be expressed as a sum of the DPE value (a catalyst property independent of the reaction of interest), the energy gained by reacting the free proton with gaseous CH_3OH to form a cationic gaseous analogue of the TS (ΔE^{TS}_{prot}, a molecular property that is catalyst-independent), and the interaction energy of the TS cation with the conjugate POM anion (E^{TS}_{int}) (Scheme 2)

$$\Delta E^{TS} = \mathrm{DPE} + \Delta E^{TS}_{prot} + E^{TS}_{int} \quad (10)$$

For materials with known structure, the DPE values (eq 1) and the other two terms in eq 10 can be obtained from DFT calculations of the structurally relaxed species involved in this cycle; ΔE^{TS}_{prot} values depend on the energies of the free proton (E^{H^+}), the gaseous TS cation obtained from transition state calculations[20,21] in the absence of a conjugate anion ($E^{TS^+(g)}$), and two gaseous CH_3OH molecules

$$\Delta E^{TS}_{prot} = E^{TS^+(g)} - E^{H^+} - 2E^{CH_3OH(g)} \quad (11)$$

E^{TS}_{int} values depend, in turn, on the energies of the ion-pair TS (E^{TS}), the gaseous TS cation ($E^{TS^+(g)}$), and the isolated conjugate anion (E^{A^-})

$$E^{TS}_{int} = E^{TS} - E^{TS^+(g)} - E^{A^-} \quad (12)$$

dx.doi.org/10.1021/ja506149c | J. Am. Chem. Soc. 2014, 136, 15229−15247

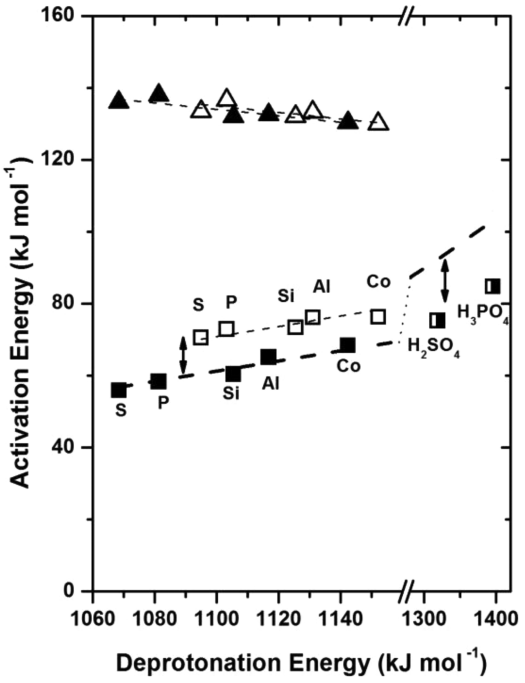

Figure 6. Calculated activation energies for DME formation from monomers and gaseous CH_3OH molecules (closed squares, open squares, half-open squares) and from protonated dimers (closed triangles, open triangles) on $H_{8-n}X^{n+}W_{12}O_{40}$ (closed symbols) and $H_{8-n}X^{n+}Mo_{12}O_{40}$ (open symbols) POM clusters and $H_{8-n}X^{n+}{}_2O_4$ gaseous mineral acids (half-open symbols) as a function of their DPE (X^{n+} = S^{6+}, P^{5+}, Si^{4+}, Al^{3+}, Co^{2+}). Protonated dimers were not stable on mineral acids. Dashed lines reflect best linear regression fits with identical slopes assumed for W-POM and Mo-POM clusters. W-POM trend lines are extrapolated to compare with mineral acids at their DPE values. Vertical arrows reflect offsets between energies on W-POM and those on other compositions.

The effect of DPE on TS formation energies (Figure 4b) for clusters with different central atoms reflects the independent DPE sensitivities of each term in eq 10 (and of corresponding steps in the thermochemical cycle, Scheme 2)

$$\frac{d\Delta E^{TS}}{dDPE} = 1 + \frac{dE_{int}^{TS}}{dDPE} \quad (13)$$

The term corresponding to $d\Delta E_{prot}^{TS}/dDPE$ is rigorously zero because ΔE_{prot}^{TS} (−815 kJ mol^{-1}; eq 11) is a property of a gaseous species and thus independent of any catalyst properties. The value of $d\Delta E^{TS}/dDPE$ is less than unity (0.29; Figure 5b and Table 2) and reflects how DPE influences the interaction energy of the TS with its conjugate POM anion ($E_{int}^{TS} < 0$), which becomes more negative as acids weaken ($dE_{int}^{TS}/dDPE < 0$), thus attenuating the effects of DPE on the formation energy of the TS (i.e., $d\Delta E^{TS}/dDPE < 1$); such attenuations are similar for W and Mo POM ($d\Delta E^{TS}/dDPE = 0.29 \pm 0.06$ for both; thus, $dE_{int}^{TS}/dDPE_{Mo\text{-}POM} \approx dE_{int}^{TS}/dDPE_{W\text{-}POM}$ from eq 13). For a given DPE value, however, ΔE^{TS} values are larger on Mo than those on W POM ($\Delta E_{Mo\text{-}POM}^{TS} - \Delta E_{W\text{-}POM}^{TS} = 15 \pm 3$; Figure 5b and Table 2) but smaller on mineral acids than the ΔE^{TS} values predicted on the basis of W-POM trends ($\Delta E_{mineral\ acid}^{TS} - \Delta E_{W\text{-}POM}^{TS} = -39 \pm 3$; Figure 5b and Table 2). These findings suggest that TS cations are less effectively stabilized (interaction energy is less negative) on Mo than on W POM anions ($E_{int,Mo\text{-}POM}^{TS} > E_{int,W\text{-}POM}^{TS} > E_{int,mineral\ acid}^{TS}$ at the same DPE, from eq 10).

The thermochemical cycle shown in Scheme 2 describes the TS formation energies in terms of interactions of protons (DPE) and of TS cations (E_{int}^{TS}) with the same conjugate anion. Such interactions between ions consist of an ionic component that reflects classical electrostatic forces as isolated ions reach interacting distances[36] and a covalent component that reflects stabilization through electronic and structural reorganizations and the sharing of electrons between neighbors in the ion pair[37,38] (shown in Scheme 2 using dotted and dashed arrows, respectively). The O−H bonds in Brønsted acids are stabilized by strong covalent interactions and by ionic stabilization that is weaker than its covalent counterpart,[9] as previously interpreted from measured potential energy profiles for the dissociation of O−H bonds (derived from O−H stretching frequencies and their overtones)[33] and from theoretical analyses of the hybridization of their molecular orbitals.[9] In contrast, the transition states in acid-catalyzed reactions exist as ion pairs[10,9,33] (consistent with +0.9 e Bader charge on the TS in Figure 3), for which ionic interactions are expected to prevail over their covalent counterparts.

The prevalence of covalent stabilization in O−H species in Brønsted acids and of electrostatic interactions at TS structures stabilized by such acids may account for the observed differences among the formation energies of surface species and among activation energies on Mo-POM, W-POM, and mineral acids (Figures 5 and 6). We surmise, based on the covalent/ionic nature of interactions in the relevant species, that protons may form O−H bonds with a greater covalent stabilization on Mo-POM than on W-POM anions; such covalency is disrupted upon proton removal (i.e., in DPE), but not recovered in essentially ionic TS structures,[9,33] leading to less negative TS formation energies than those expected from DPE values on Brønsted acids with more covalent O−H bonds. Similarly, a less covalent O−H bonds in mineral acids (relative to POM clusters) may account for the more negative TS energies on mineral acids compared with those predicted for their DPE values from the trends observed in W-POM clusters (Figures 5 and 6). Next, we test this hypothesis by dissecting DPE values and TS−anion interaction energies (E_{int}^{TS}) into their ionic and covalent components and incorporating them in thermochemical cycles that describe TS formation energies (Scheme 2) on W and Mo POM clusters and mineral acids.

3.3. Ionic and Covalent Contributions to O−H Bonds and DPE Values for Brønsted Acids. DPE values for O−H bonds in Brønsted acids can be dissected into their ionic ($E_{ion}^{H^+}$) and covalent (E_{cov}^{H+}) components

$$DPE = E_{ion}^{H^+} + E_{cov}^{H+} \quad (14)$$

The classical electrostatic interaction energies between a proton and the DFT-derived charge distribution of a structurally relaxed isolated POM anion ($E_{es}^{H^+}$; eq 2) are first calculated as a function of the proton−anion distance (without relaxing the electron distribution in the anion in response to its interaction with the proton). These interaction energies become more negative with decreasing distance, reach a minimum value, and then increase again (Figure 7a), as expected for interactions between opposite charges.[36] The proton−anion distance for $E_{es}^{H^+}$ minima ($E_{es,min}^{H^+}$) depends on the anion size because overlap between the proton and the diffuse electron cloud of the anion (Scheme 3 and Figure 7) causes incipient repulsion by the nuclear point charges. The proton−anion distances at energy minima are similar on all POM clusters (0.15 to 0.16 nm; Figure 7a)

dx.doi.org/10.1021/ja506149c | J. Am. Chem. Soc. 2014, 136, 15229−15247

Scheme 2. A Thermochemical Cycle Accounting for the Thermodynamic Properties of the DME Formation Transition State (ΔE^{TS}) in Terms of the DPE of the Acid (HA), the Energy To Form a Gaseous TS Cation from a Free Proton (ΔE^{TS}_{prot}), and the Interaction Energy (E^{TS}_{int}) of TS Cation with the Conjugate Anion (A^-)[a]

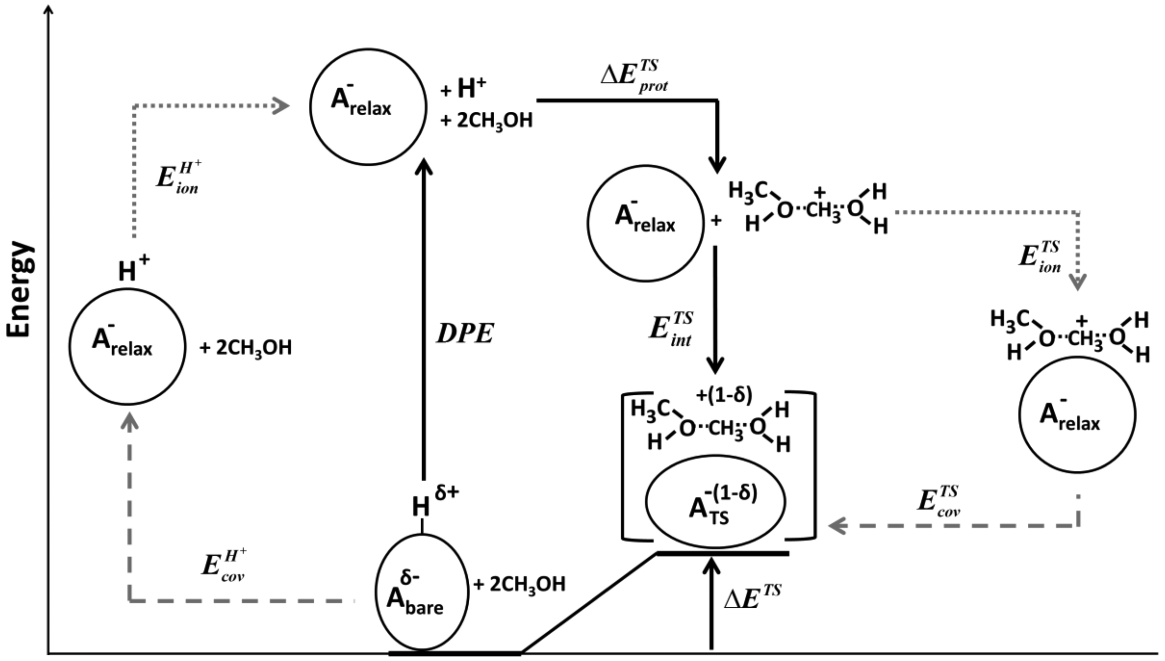

[a] H^+ and A^- represent the proton and the anion of a POM cluster, respectively. Solid arrows reflect total interaction energies, whereas dotted and dashed arrows reflect their ionic and covalent components, respectively. Analogous thermochemical cycles for monomer and dimer intermediates are shown in the Supporting Information (Schemes S2 and S3).

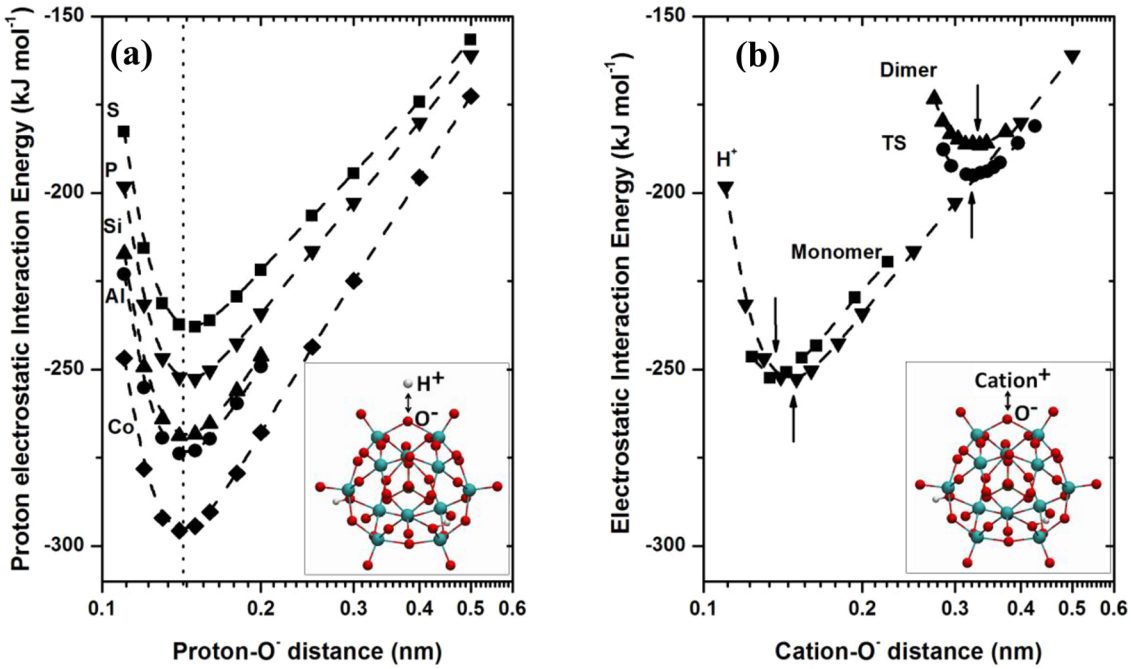

Figure 7. Electrostatic interaction energies of (a) a proton with $[H_{7-n}X^{n+}W_{12}O_{40}]^-$ POM anions (X^{n+} = S^{6+}, P^{5+}, Si^{4+}, Al^{3+}, Co^{2+}) and of (b) proton, monomer, protonated dimer and TS cations with $[H_2PW_{12}O_{40}]^-$ anion as a function of cation−anion distance. Anion positions are taken as those of the O^- atom from which an H^+ is removed. Cation positions are taken as those of the removed H^+ for all cations except the TS; the TS cation position is at the C atom of the CH_3^+ structure. The dotted line and vertical arrows reflect distances of the most negative electrostatic interaction energies.

due to the similar size and spatial charge distribution of all POM anions. Cations (Figure 7b) and anions (Supporting Information, Figure S3; HX with X = F, Cl, Br, I) of different sizes incipiently overlap their charge distributions at different distances, leading to concomitant differences in their "equilibrium" distances for unrelaxed charge distributions in the anions. The $E^{H^+}_{es,min}$ values reflect the most stable configuration for H^+−anion pairs when the latter retain the electronic distribution of the

dx.doi.org/10.1021/ja506149c | J. Am. Chem. Soc. 2014, 136, 15229−15247

Scheme 3. Surfaces of Constant Charge Density (at 200 e nm $^{-3}$) for Protons and Structurally Relaxed Gaseous Cationic Analogues of Monomers, Dimers, and Transition States; for $[H_2PW_{12}O_{40}]^-$ Anions (Left; Ions Are Placed at Cation–Anion Distances of Most Favorable Electrostatic Interactions as Shown by Vertical Arrows in Figure 7b); and for Their Respective Structurally Relaxed Neutral Structures (Right)[a]

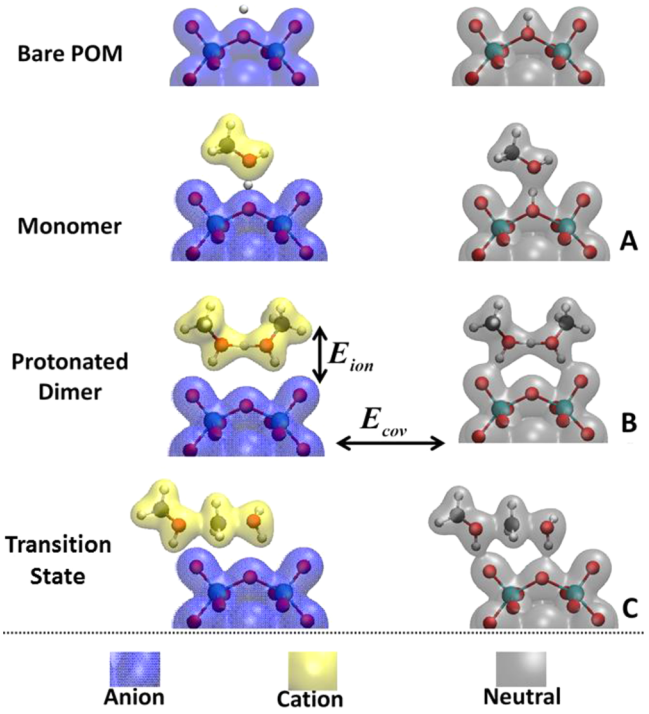

[a]Electrostatic interaction between ions at shown distances (left) reflect ionic components while subsequent relaxations to form stable surface intermediates (right) reflect covalent components of interaction energies. Structures A, B, and C correspond to those in Figure 3.

isolated anion. We define the ionic component of DPE ($E_{ion}^{H^+}$) as the energy required to overcome such electrostatic interactions between the proton and the unrelaxed anion

$$E_{ion}^{H^+} = -E_{es,min}^{H+} \quad (15)$$

The covalent component ($E_{cov}^{H^+}$) reflects contributions from relaxations of the anion and is given by the difference between DPE and $E_{ion}^{H^+}$ values (eq 14).

The ionic component of DPE ($E_{ion}^{H^+}$) on W and Mo POM (Table 3 and Figure 8; 238–296 and 246–289 kJ mol $^{-1}$, respectively) are much smaller but change more significantly than their covalent ($E_{cov}^{H^+}$) counterparts (830–847 and 853–863 kJ mol $^{-1}$, respectively) on clusters with different central atoms. These linear changes in $E_{ion}^{H^+}$ values with a central atom (Figure 8) give rise to the linearity of rates and activation energies with DPE (Figures 5 and 6). $E_{cov}^{H^+}$ values much larger than E_{ion}^{H+} are consistent with the known covalent nature of O–H bonds in solid acids[9,33] and with Fajans' rules.[37,38] These values illustrate how interactions between small cations (proton, point charge) and large anions (POM, ~1.2 nm) tend to be more covalent than those between larger cations and smaller anions, as a consequence of the more polarizing nature of smaller cations and the more polarizable character of larger anions.[37,38] Gaseous sulfuric and phosphoric acid moieties have smaller $E_{cov}^{H^+}$ values (Table 3 and Figure 8; 724 and 723 kJ mol $^{-1}$) than POM clusters because of their smaller HSO_4^- and $H_2PO_4^-$ conjugate anions. The E_{ion} and E_{cov} estimates for molecular systems (LiCl, HCl, CH_4) are also consistent with the expected covalent character of their bonds (Supporting Information, Table S1; $E_{cov,Li^+-Cl^-} < E_{cov,H^+-Cl^-} < E_{cov,H^+-CH_3^-}$), suggesting that the treatment that we propose here (eqs 14 and 15) provides an accurate assessment of the ionic and covalent components in interacting ions.

For POM clusters with either W or Mo addenda atoms, changes in DPE values for different central atoms reflect concomitant changes in both covalent and ionic components. The ionic component, however, increased more sharply than the covalent one with increasing DPE values (Figure 8a; $dE_{ion}^{H^+}/dDPE$ = 0.75 ± 0.08, ionic; Figure 8b; $dE_{cov}^{H^+}/dDPE$ = 0.25 ± 0.08, covalent) for both Mo and W POM clusters. Mo-POM clusters have larger $E_{cov}^{H^+}$ values and smaller $E_{ion}^{H^+}$ values than those for W-POM clusters for a given DPE value (Figure 8; $E_{cov,Mo\text{-}POM}^{H^+} - E_{cov,W\text{-}POM}^{H^+}$ = 16 ± 4 kJ mol $^{-1}$). The size of W and Mo POM

Table 3. Calculated Deprotonation Energies (DPE), Their Ionic and Covalent Components (E_{ion}^{H+} and E_{cov}^{H+}), Bader Charges on Central Tetrahedra ($q_{X^{n+}O_4}^{neutral}$ and $q_{X^{n+}O_4}^{anion}$) and Metal-Oxide Shells ($q_{H_{8-n}M_{12}O_{36}}^{neutral}$ and $q_{H_{8-n}M_{12}O_{36}}^{anion}$) of Neutral Clusters and of Structurally Relaxed Conjugate Anions, and Displacements of the Center of Charge upon Relaxation of the Unrelaxed Conjugate Anions ($|\langle\vec{r}_a^{unrel}\rangle - \langle\vec{r}_a^{rel}\rangle|$; eq 3) for POM Clusters and Mineral Acids in the Gas Phase[a]

composition	DPE	E_{ion}^{H+}	E_{cov}^{H+}	$q_{X^{n+}O_4}^{neutral}$ (e)	$q_{H_{8-n}M_{12}O_{36}}^{neutral}$ (e)	$q_{X^{n+}O_4}^{anion}$ (e)	$q_{H_{8-n}M_{12}O_{36}}^{anion}$ (e)	$\lvert\langle\vec{r}_a^{unrel}\rangle - \langle\vec{r}_a^{rel}\rangle\rvert$ (Å)
$H_2S^{6+}W$	1068	238	830	−1.75	1.75	−1.75	0.75	4.16
$H_3P^{5+}W$	1081	253	829	−2.44	2.44	−2.45	1.45	4.15
$H_4Si^{4+}W$	1105	269	837	−3.09	3.09	−3.11	2.11	4.20
$H_5Al^{3+}W$	1117	274	843	−3.71	3.71	−3.73	2.73	4.25
$H_6Co^{2+}W$	1142	296	847	−4.11	4.11	−4.11	3.11	4.36
$H_2S^{6+}Mo$	1095	242	853	−1.73	1.73	−1.73	0.73	4.35
$H_3P^{5+}Mo$	1103	253	850	−2.39	2.39	−2.39	1.39	4.29
$H_4Si^{4+}Mo$	1125	267	858	−2.96	2.96	−2.98	1.98	4.36
$H_5Al^{3+}Mo$	1131	269	862	−3.44	3.44	−3.46	2.46	4.40
$H_6Co^{2+}Mo$	1152	289	863	−3.37	3.37	−3.38	2.38	4.52
$H_2S^{6+}O_4(g)$	1319	595	724	−2	2	−2	1	1.74
$H_3P^{5+}O_4(g)$	1395	672	723	−3	3	−3	2	1.70

[a]All energies are in kJ mol $^{-1}$.

dx.doi.org/10.1021/ja506149c | J. Am. Chem. Soc. 2014, 136, 15229–15247

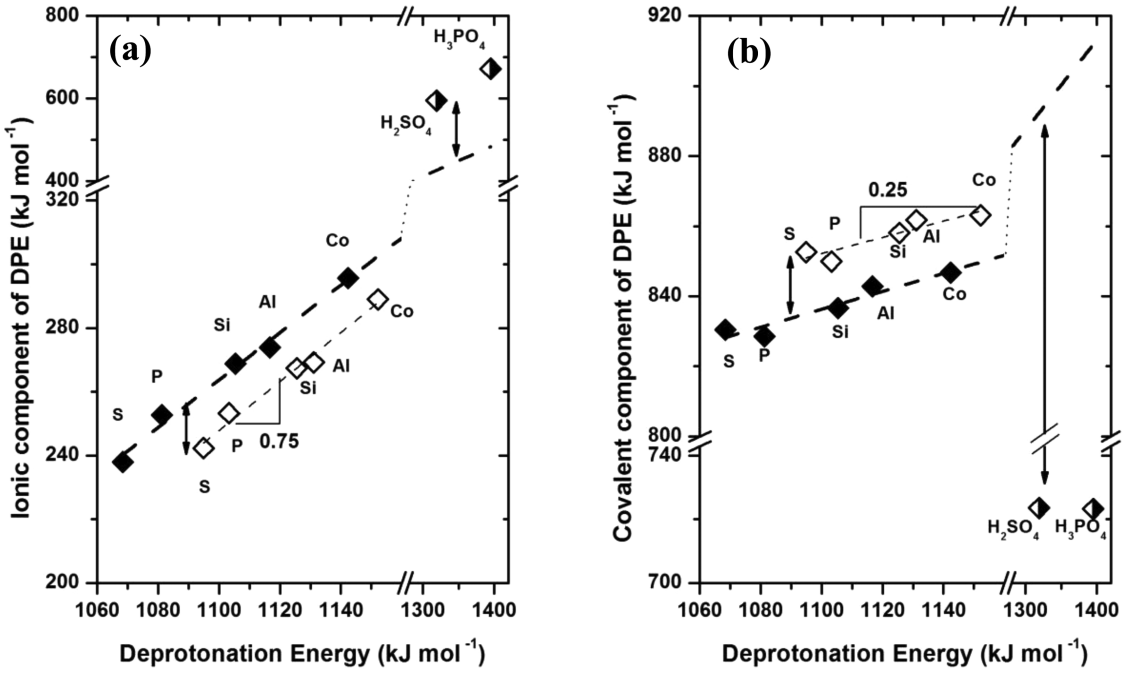

Figure 8. Ionic (a) and covalent (b) components of DPE for $H_{8-n}X^{n+}W_{12}O_{40}$ (closed symbols), $H_{8-n}X^{n+}Mo_{12}O_{40}$ (open symbols) POM clusters, and $H_{8-n}X^{n+}{}_2O_4$ gaseous mineral acids (half-open symbols) as a function of their DPE (X^{n+} = S^{6+}, P^{5+}, Si^{4+}, Al^{3+}, Co^{2+}). Dashed lines reflect best linear regression fits, with identical slopes assumed for W-POM and Mo-POM clusters. W-POM trend lines are extrapolated to compare with mineral acids at their DPE values. Vertical arrows reflect offsets between energies on W-POM and those on other compositions.

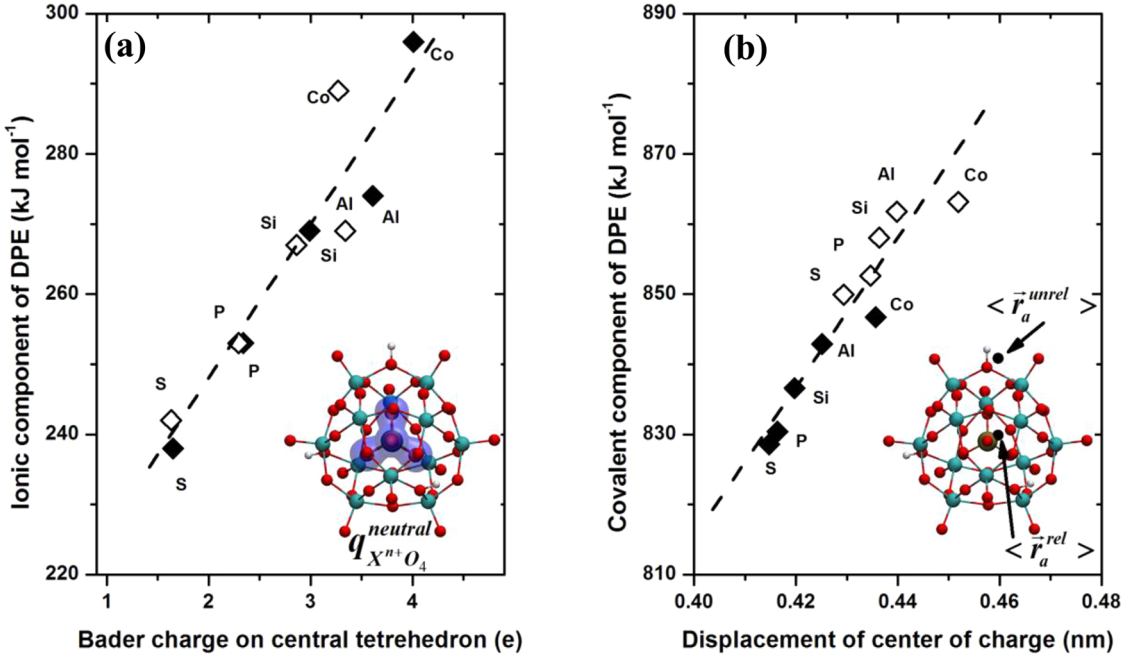

Figure 9. (a) Ionic component of DPE as a function of the Bader charge on central POM tetrahedron ($q^{neutral}_{X^{n+}O_4}$) and (b) covalent component of DPE as a function of displacement of the center of anion charge upon deprotonation ($|\langle \vec{r}_a^{unrel} \rangle - \langle \vec{r}_a^{rel} \rangle|$ calculated using eq 3) for $H_{8-n}X^{n+}W_{12}O_{40}$ (closed symbols) and $H_{8-n}X^{n+}Mo_{12}O_{40}$ (open symbols) POM clusters (X^{n+} = S^{6+}, P^{5+}, Si^{4+}, Al^{3+}, Co^{2+}). The $q^{neutral}_{X^{n+}O_4}$ and $|\langle \vec{r}_a^{unrel} \rangle - \langle \vec{r}_a^{rel} \rangle|$ quantities are reporters of the extent of charge localization near the center of POM clusters and of the extent of charge reorganization throughout the outer shell when clusters are deprotonated, respectively.

clusters is similar and independent of the central atom (~1.2 nm), indicating that these different relative magnitudes of the ionic and covalent components of DPE reflect instead different intracluster electronic distributions.

Next, we examine charge distributions in central tetrahedra and octahedral shells in POM clusters and the extent to which they reorganize upon deprotonation. The ionic component of DPE ($E^{H^+}_{ion}$) on Mo and W POM clusters correlates with estimates of Bader charges[28,29] on the $(X^{n+}O_4)^{(n-8)}$ tetrahedra ($q_{X^{n+}O_4}$) at the center of these Keggin clusters (Figure 9a; Mo and W POM clusters follow the same linear trend) because $q_{X^{n+}O_4}$ values reflect charges that are localized near the center of POM anions,

dx.doi.org/10.1021/ja506149c | J. Am. Chem. Soc. 2014, 136, 15229−15247

Scheme 4. A Thermochemical Cycle Describing the TS Stability in Terms of the Ionic and Covalent Components of the TS−Anion Interaction Energy Expressed as Fractions (f_{ion}, f_{cov}) of the Respective Components of the DPE[a]

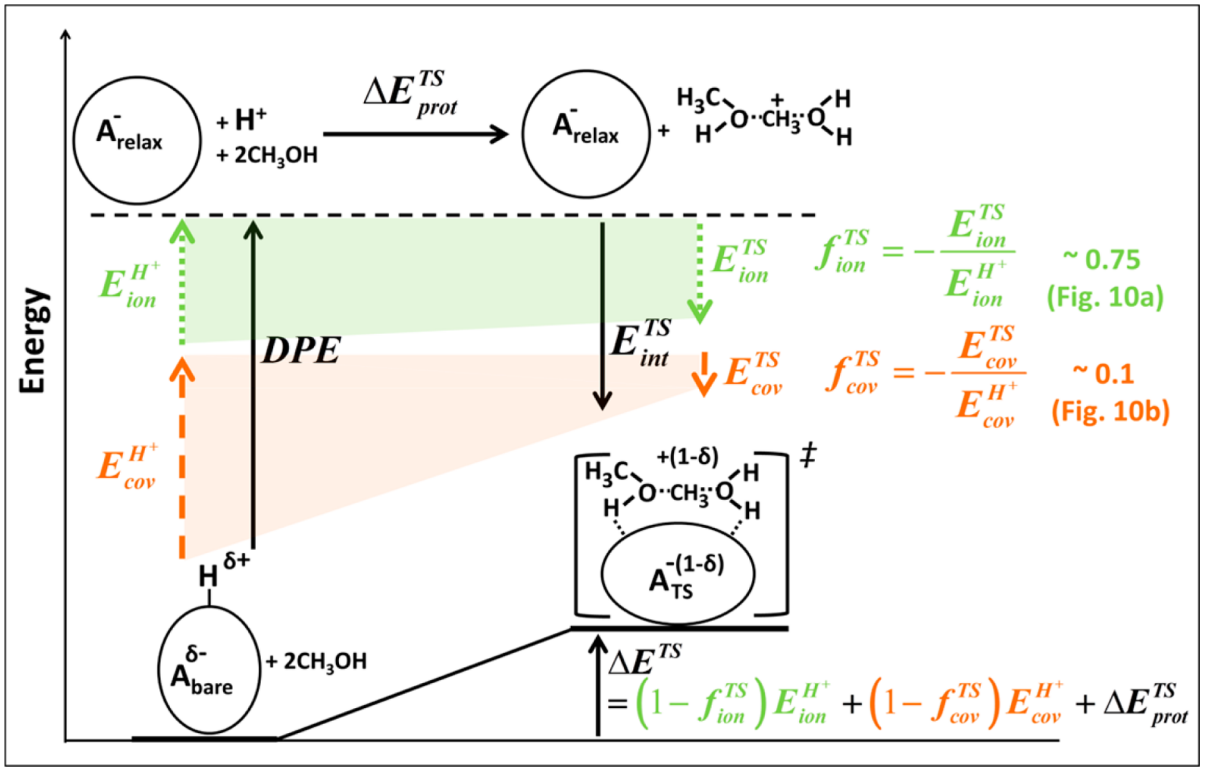

[a]Dotted and dashed arrows reflect ionic and covalent components of interactions energies, respectively, which are further illustrated in Scheme 2.

whereas their counter charges are near the charge balancing protons (acid sites) that are well-separated from each other; therefore, the proton being removed (in DPE) can interact more strongly with $q_{X^{n+}O_4}$ than with counter charges at vicinal protons. The $(S^{6+}O_4)^{2-}$ tetrahedron in a neutral $H_2SW_{12}O_{40}$ cluster has a $q^{neutral}_{X^{n+}O_4}$ value of −1.75 e (Table 3), whereas the cationic $(H_2W_{12}O_{36})^{2+}$ shell has a +1.75 e charge (making the overall cluster neutral), suggesting that $(SO_4)^{2-}$ delocalizes the residual −0.25 e of its −2 e formal charge via interactions with the oxide shell. The $q^{neutral}_{X^{n+}O_4}$ values increase more weakly than the formal charge for tetrahedra with different central atoms (n − 8 for $X^{n+}O_4$). The $q^{neutral}_{X^{n+}O_4}/(n-8)$ ratio decreases from 0.87 on SO_4^{2-} to 0.69 on CoO_4^{-6} (Table 3) because highly charged tetrahedra interact more strongly with the oxide shell and delocalize a larger fraction of their charge than less charged tetrahedra. The charges on central tetrahedra are of similar magnitude for neutral POM clusters and their anions ($q^{neutral}_{X^{n+}O_4} \approx q^{anion}_{X^{n+}O_4}$; Table 3), consistent with highly localized central charges that remain unperturbed by interactions with protons located at the outer oxide shell.

The covalent component of DPE ($E^{H^+}_{cov}$) on POM clusters reflects the extent of charge reorganization upon deprotonation, which can be quantified by the displacement of the center of charge in converting the neutral clusters to the conjugate anions ($|\langle \vec{r}^{unrel}_a \rangle - \langle \vec{r}^{rel}_a \rangle|$;[30] Figure 9b). The center of charge (eq 3) was first calculated using the same anion charge distribution as that derived from DFT for a neutral cluster, but without including the proton ($\langle \vec{r}^{unrel}_a \rangle$), and then using the charge distribution of the structurally relaxed anion ($\langle \vec{r}^{rel}_a \rangle$). The $\langle \vec{r}^{unrel}_a \rangle$ position lies very near the original location of the proton in the neutral cluster (~0.1 nm; inset in Figure 9b), but the relaxation moves it close to the central atom ($\langle \vec{r}^{rel}_a \rangle$), suggesting that the negative charge reorganizes throughout the oxide shell but not through the central tetrahedron because $q_{X^{n+}O_4}$ is unchanged by deprotonation (Table 3). A visualization of the charge density difference between deprotonated and neutral clusters (Supporting Information, Figure S7) shows a depletion of electron density at the location where proton used to be and an accumulation at all O atoms in the oxide shell, including the terminal O atoms, consistent with such reorganization. The values of $E^{H^+}_{cov}$ and $|\langle \vec{r}^{unrel}_a \rangle - \langle \vec{r}^{rel}_a \rangle|$ depend very weakly on the identity of the central atom (Figure 9b and Table 3), indicating that more highly charged oxide shells around a central atom of lower valence reorganize the anion charge over longer distances than shells of lower charge, making the latter exhibit more covalent character in their O−H bonds. Consistent with the effect of addenda atoms on $E^{H^+}_{cov}$ (Figure 8), the $|\langle \vec{r}^{unrel}_a \rangle - \langle \vec{r}^{rel}_a \rangle|$ values are indeed larger on Mo than on W POM clusters for the same central atoms (Figure 9b and Table 3). These more extensive charge reorganizations on Mo-POM are also consistent with their lower energy gaps than W-POM clusters ($E_{HOMO-LUMO,HPMo}$ = 2.5 eV, $E_{HOMO-LUMO,HPW}$ = 3.3 eV from UV−visible spectra[15]), in light of the expected inverse relation between the polarizability of metal oxides and their HOMO−LUMO gaps.[39]

This analysis of charge localization and reorganization leads us to conclude that central atoms in POM clusters affect the ionic component of DPE to a greater extent than the covalent component because of their greater charge localization near central atoms of lower valence, whereas addenda atoms (Mo, W) affect the covalent component of DPE ($E^{H^+}_{cov,MO\text{-}POM} > E^{H^+}_{cov,W\text{-}POM}$) because MoO_x shells can reorganize charge more effectively than their WO_x analogues.

Next, we consider how the ionic and covalent contributions to DPE values in Mo and W POM clusters and mineral acids influence the extent to which neutral and cationic intermediates and

dx.doi.org/10.1021/ja506149c | J. Am. Chem. Soc. 2014, 136, 15229−15247

Table 4. Calculated Interaction Energies of Gaseous Cations of Monomers (E_{int}^{mono}), Protonated Dimers (E_{int}^{dimer}), and Transition States (E_{int}^{TS}) with Conjugate Anions on POM Clusters and Mineral Acids and Ionic (E_{ion}^{mono}, E_{ion}^{dimer}, and E_{ion}^{TS}, Respectively) and Covalent (E_{cov}^{mono}, E_{cov}^{dimer}, and E_{cov}^{TS}, Respectively) Components of Such Interaction Energies[a]

composition	E_{int}^{mono}	E_{ion}^{mono}	E_{cov}^{mono}	E_{int}^{dimer}	E_{ion}^{dimer}	E_{cov}^{dimer}	E_{int}^{TS}	E_{ion}^{TS}	E_{cov}^{TS}
HSW	−959	−241	−718	−297	−178	−119	−270	−187	−83
HPW	−972	−252	−720	−310	−186	−123	−281	−195	−86
HSiW	−992	−270	−722	−322	−192	−130	−299	−205	−94
HAlW	−1002	−267	−735	−327	−192	−135	−304	−205	−99
HCoW	−1021	−291	−731	−341	−207	−135	−320	−220	−100
HSMo	−975	−241	−735	−296	−178	−122	−272	−186	−86
HPMo	−985	−251	−734	−307	−181	−126	−280	−191	−88
HSiMo	−1003	−266	−737	−319	−188	−132	−297	−201	−96
HAlMo	−1009	−264	−745	−324	−188	−136	−300	−202	−98
HCoMo	−1025	−287	−738	−337	−199	−138	−317	−213	−103
H_2SO_4(g)	−1189	−555	−615	−503			−477	−388	−89
H_3PO_4(g)	−1257	−639	−618	−581			−540	−393	−144

[a]All energies are in kJ mol $^{-1}$.

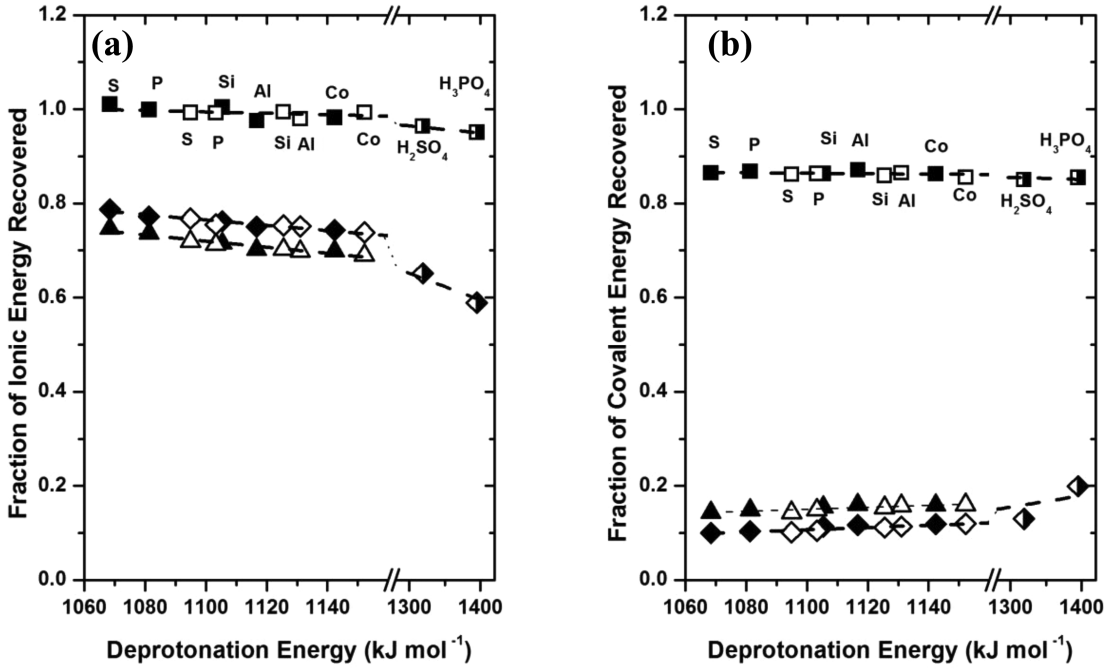

Figure 10. Fractions of (a) ionic (f_{ion}; eq 17) and (b) covalent (f_{cov}; eq 18) components of DPE, recovered by interactions of monomer (closed squares, open squares, half-open squares), protonated dimer (closed triangles, open triangles), and transition state (closed diamonds, open diamonds, half-open diamonds) cations with conjugate anions on $H_{8-n}X^{n+}W_{12}O_{40}$ (closed symbols) and $H_{8-n}X^{n+}Mo_{12}O_{40}$ (open symbols) POM clusters and $H_{8-n}X^{n+}{}_2O_4$ gaseous mineral acids (half-open symbols) as a function of DPE (X^{n+} = S^{6+}, P^{5+}, Si^{4+}, Al^{3+}, Co^{2+}). Protonated dimers were not stable on mineral acids. The dashed lines reflect best regression fits to the forms of eqs 19 and 20; their corresponding regressed parameters are shown in Table 5.

transition states are stabilized by conjugate anions (Scheme 4), and in doing so, we develop a general framework to describe compositional consequences for CH_3OH dehydration activation energies.

3.4. Ionic and Covalent Contributions to Interaction Energies of TS, Monomer, and Dimer Cations with Conjugate Anions. As in the case of DPE, the interaction energies of cationic TS structures with their conjugate anions (E_{int}^{TS}) can be dissected into their ionic (E_{ion}^{TS}) and covalent (E_{cov}^{TS}) components (dotted and dashed arrows in Scheme 2, respectively)

$$E_{int}^{TS} = E_{ion}^{TS} + E_{cov}^{TS} \quad (16)$$

The minimum values of electrostatic interaction energies of the TS cation (E_{es}^{TS}; Figure 7b) represent the ionic components of these interaction energies ($E_{ion}^{TS} = E_{es,min}^{TS}$; analogous to eq 15); the covalent component that reflects electronic and structural relaxation (as shown in Scheme 3) is then given by the difference between E_{int}^{TS} and E_{ion}^{TS} (eq 16).

For a given acid, the effects of ionic and covalent interactions on energies of monomers and dimers that act as references for the activation energies (E_a^{mono}, E_a^{dimer}; eqs 8 and 9) are best understood by the use of thermochemical cycles analogous to the one used to describe TS energies in Scheme 2 and eq 10 (Supporting Information, Schemes S2 and S3). These cycles express formation energies of respective species in terms of the acid DPE, the reaction energy of a free proton with one or two CH_3OH(g) molecules to form a gaseous monomer or dimer cation (ΔE_{prot}^{mono}, ΔE_{prot}^{dimer}), and the interaction energies of such cations (E_{int}^{mono}, E_{int}^{dimer}) with the conjugate anions. The E_{int}^{mono} and

dx.doi.org/10.1021/ja506149c | J. Am. Chem. Soc. 2014, 136, 15229−15247

Table 5. Electrostatic Interaction Energies of the Gaseous CH_3OH Monomers with a Proton (ΔE_{prot}^{mono}); Formation Energies of Gaseous Cations of Protonated Dimers (ΔE_{prot}^{dimer}) and Transition States (ΔE_{prot}^{TS}); and Fractions of the Ionic ($f_{ion,1000}$) and Covalent ($f_{cov,1000}$) Components of DPE Recovered by Interactions of Monomer, Protonated Dimer, and Transition State Cations with Conjugate Anions at a DPE Value of 1000 kJ mol^{-1} and Their Linear Dependences on DPE (α_{ion} and α_{cov})[a]

	ΔE_{prot} (kJ mol^{-1})	$f_{ion,1000}$[b]	α_{ion}[b] (10^{-4} kJ^{-1} mol)	$f_{cov,1000}$[c]	α_{cov}[c] (10^{-4} kJ^{-1} mol)
monomer	−182	1.01 (±0.01)	−1.5 (±0.5)	0.87 (±0.005)	−0.4 (±0.3)
dimer	−924	0.79 (±0.02)	−6.5 (±1.4)	0.13 (±0.01)	2.1 (±1.0)
TS	−815	0.82 (±0.01)	−5.7 (±0.4)	0.08 (±0.01)	2.4 (±0.8)

[a]These quantities represent catalyst-independent properties of reactive species that are needed to describe their stability. [b,c]Obtained by regression of f_{ion} and f_{cov} values shown in Figure 10 to the forms of eqs 19 and 20, respectively.

E_{int}^{dimer} values can be dissected into ionic and covalent components in the same manner as that for E_{int}^{TS} values (eq 16). The structure, charge distribution, and energy of the cationic gaseous analogue of protonated dimers were obtained from structurally relaxed DFT calculations as in the case of TS cations (eq 12). CH_3OH monomers, however, are uncharged CH_3OH molecules H-bonded to protons instead of $CH_3OH_2^+$ cations; therefore, the monomer cation was approximated as an isolated proton stabilized only by electrostatic dipole interaction from a neutral CH_3OH placed at a distance of most negative interaction energy with it (0.13 nm O_{M1}−H_{C1} distance).

Table 4 shows the interaction energies of monomer, dimer, and TS cations (E_{int}) with anions formed by deprotonating POM clusters and mineral acids and the ionic (E_{ion}) and covalent (E_{cov}) components of these interactions energies. These E_{int}^{mono}, E_{int}^{dimer}, and E_{int}^{TS} values reflect the stabilization of the respective cations ($E_{int} < 0$; Table 4), which recovers some of the energy required to deprotonate the acid in the form of the ionic and covalent interactions of these species with the conjugate anion ($|E_{int}| <$ DPE; Tables 3 and 4 and Schemes 2 and 4). The strength of ionic interactions depends inversely on the cation−anion distance (eq 2; $E_{es} \sim 1/r_{ac}$); as a result, small cations (protons and monomers) show stronger ionic interactions than larger cations (dimer and TS cations). The more polarizing nature of smaller cations[37,38] also induces more extensive charge reorganization (covalent stabilization) in a given conjugate anion. Consequently, both ionic and covalent DPE components are larger than the corresponding ionic and covalent components of interaction energies of reactive intermediates and transition states with conjugate anions ($|E_{ion}^{H^+}| \approx |E_{ion}^{mono}| > |E_{ion}^{dimer}|, |E_{ion}^{TS}|$; $|E_{cov}^{H^+}| > |E_{cov}^{mono}| \gg |E_{cov}^{dimer}|, |E_{cov}^{TS}|$; Tables 3 and 4) because a proton is the smallest cation.

Figure 10 shows the ionic and covalent components of interaction energies of TS cation (E_{ion}^{TS}, E_{cov}^{TS}) expressed as fractions (f_{ion}^{TS},f_{cov}^{TS}; illustrated in Scheme 4) of the respective components for protons, reflected in their DPE values ($E_{ion}^{H^+}$, $E_{cov}^{H^+}$)

$$f_{ion}^{TS} = -\frac{E_{ion}^{TS}}{E_{ion}^{H^+}} \quad (17)$$

$$f_{cov}^{TS} = -\frac{E_{cov}^{TS}}{E_{cov}^{H^+}} \quad (18)$$

and for monomer (f_{ion}^{mono}, f_{cov}^{mono}) and protonated dimer (f_{ion}^{dimer}, f_{cov}^{dimer}) cations, similarly defined, as a function of the DPE of Mo and W POM clusters and mineral acids. These fractions are single-valued functions of DPE (described by a single trend line) for Mo and W POM and mineral acids (Figure 10). Higher DPE values coincide with smaller f_{ion} values and larger f_{cov} values, indicating that organic cations become more covalently stabilized relative to protons for weaker acids. These effects can be empirically described by the weak linear dependence of f_{ion}^{TS} and f_{cov}^{TS} on DPE evident from the results shown in Figure 10

$$f_{ion}^{TS} = f_{ion,1000}^{TS} + \alpha_{ion}^{TS}(\text{DPE} - 1000) \quad (19)$$

$$f_{cov}^{TS} = f_{cov,1000}^{TS} + \alpha_{cov}^{TS}(\text{DPE} - 1000) \quad (20)$$

The regressed values of fractions recovered at a DPE of 1000 kJ mol^{-1} ($f_{ion,1000}^{TS}$ and $f_{cov,1000}^{TS}$) and their slopes (α_{ion}^{TS} and α_{cov}^{TS}) can then be used to obtain the relevant values of fractions for all species on Mo or W POM or mineral acids (Figure 10 and Table 5). The fractions of the DPE components recovered by monomer and dimer cations, which also show weak dependence on DPE (Figure 10), can be described by the analogs of eqs 19 and 20 using their respective f_{1000} and α values shown in Table 5.

Cationic monomers recover essentially the full ionic component and most of the covalent component of DPE values via interactions with POM conjugate anions ($f_{ion}^{mono} \approx 1$, $f_{cov}^{mono} =$ 0.86−0.87; Figure 10), consistent with their proton-like character (H^+ and a neutral CH_3OH). In contrast, protonated dimers and TS cations recover large fractions of the ionic ($f_{ion}^{TS} =$ 0.79−0.74, $f_{ion}^{dimer} =$ 0.75−0.70; Figure 10) but much smaller fractions of the covalent ($f_{cov}^{TS} =$ 0.10−0.12 and $f_{cov}^{dimer} =$ 0.14−0.16; Figure 10) components of DPE values, consistent with their larger size compared to H^+ and with their ion-pair structures on POM clusters, inferred from Bader charges (+0.90 e for TS and +0.87 e for dimer).

The ionic and covalent components of the DPE values and the fractions of each recovered via interactions of organic cations with conjugate anions to form an ion-pair TS (as described by the thermochemical cycle; Scheme 4) confirm that the different ionic and covalent nature of O−H species in different acids are responsible for the origins of the less stable nature of the TS on Mo than on W POM clusters of similar DPE (Figure 5). For a given DPE, Mo-POM clusters have larger covalent and smaller ionic DPE components than those for W-POM (Figure 8); ion pairs at the TS, irrespective of acid identity, recover much smaller fractions of the covalent ($f_{cov}^{TS} =$ 0.10−0.12; Figure 10 and Scheme 4) than the ionic ($f_{ion}^{TS} =$ 0.79−0.74; Figure 10 and Scheme 4) DPE components, making such ion pairs less stable on acids with higher covalency at a given DPE (Mo-POM). Similarly, the smaller covalent component of DPE on mineral acids (Figure 8) accounts for the more stable TS structures than expected based on the trends established for W-POM clusters. Monomer and dimer cations also recover smaller fractions of covalent than of ionic components (Figure 10), which explains (using treatments analogous to TS) why these intermediates are less stable on acids with a larger covalent component of DPE at similar DPE values.

Next, we incorporate the ionic and covalent components of these interaction energies into the thermochemical cycles to

dx.doi.org/10.1021/ja506149c | J. Am. Chem. Soc. 2014, 136, 15229−15247

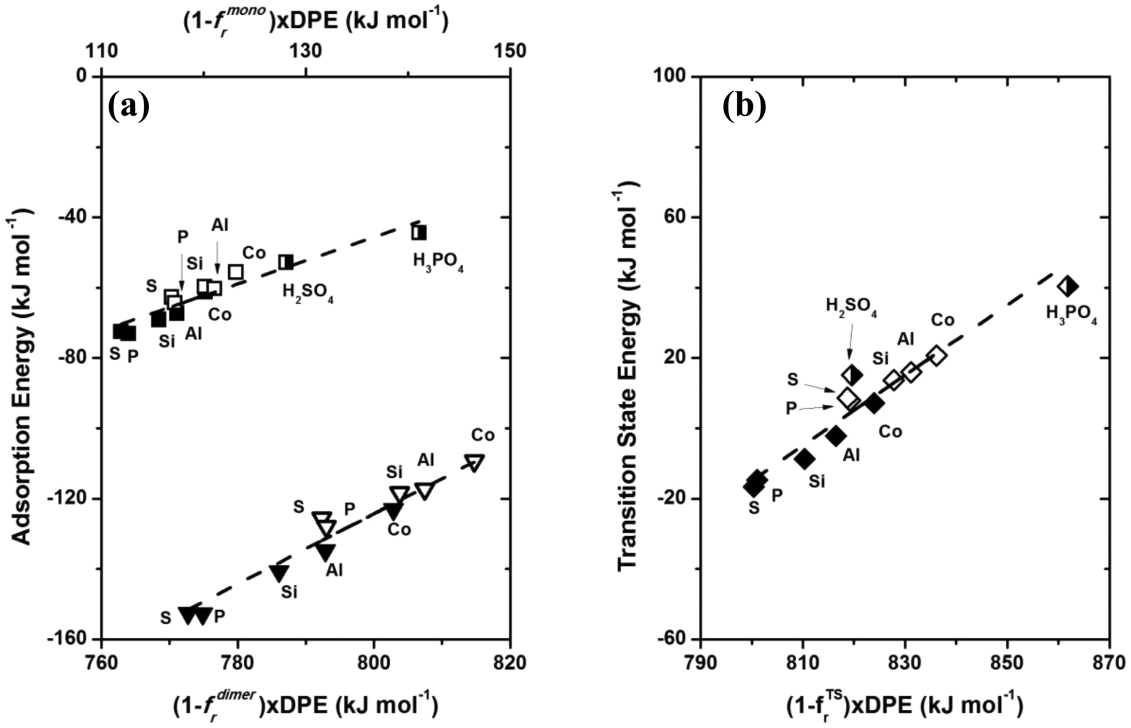

Figure 11. (a) Monomer (closed squares, open squares, half-open squares) and protonated dimer (closed triangles, open triangles) adsorption energies and (b) DME formation TS energies (closed diamonds, open diamonds, half-open diamonds) on $H_{8-n}X^{n+}W_{12}O_{40}$ (closed symbols) and $H_{8-n}X^{n+}Mo_{12}O_{40}$ (open symbols) POM clusters and $H_{8-n}X^{n+}{}_2O_4$ gaseous mineral acids (half-open symbols) as a function of $(1 - f_r) \times$ DPE values, which reflect unrecovered fractions of DPE for each species ($X^{n+} = S^{6+}$, P^{5+}, Si^{4+}, Al^{3+}, Co^{2+}). The dashed lines reflect best regression fits to eqs 23, 25, and 26; they have intercepts equal to ΔE_{prot} values (shown in Table 5) and slopes equal to unity.

develop quantitative correlations that describe the energies of reactive intermediates and TS using probe-independent (and reaction-independent) properties of acid catalysts (E_{ion}^{H+}, E_{cov}^{H+}; Table 3) and properties of reactive species that do not depend on acid identity or strength (f_{ion}, f_{cov}, and ΔE_{prot}; Table 5).

3.5. Influence of Ionic and Covalent Interactions on Stabilities of Surface Species and Activation Energies. The TS formation energy (ΔE^{TS}), as described by the thermochemical cycle in Scheme 2 and by eq 10, depends on the interaction energies of H^+ (DPE) and the TS cation (E_{int}^{TS}) with their conjugate anion, which reflect the additive contributions of their respective ionic (E_{ion}^{H+}, E_{ion}^{TS}) and covalent components (E_{cov}^{H+}, E_{cov}^{TS})

$$\Delta E^{TS} = [E_{ion}^{H+} + E_{cov}^{H+}] + \Delta E_{prot}^{TS} + [E_{ion}^{TS} + E_{cov}^{TS}] \quad (21)$$

The E_{ion}^{TS} and E_{cov}^{TS} values reflect the fractions of the DPE components (f_{ion}^{TS}, f_{cov}^{TS}, respectively; Figure 10 and Scheme 4) recovered by interactions of TS cations with their conjugate anions; substitution of these fractions (eqs 17 and 18) into eq 21 gives

$$\Delta E^{TS} = [E_{ion}^{H+} + E_{cov}^{H+}] - [f_{ion}^{TS} E_{ion}^{H+} + f_{cov}^{TS} E_{cov}^{H+}] + \Delta E_{prot}^{TS} \quad (22)$$

which can be rearranged as

$$\Delta E^{TS} = (1 - f_r^{TS})\mathrm{DPE} + \Delta E_{prot}^{TS} \quad (23)$$

Here

$$f_r^{TS} = f_{ion}^{TS} \frac{E_{ion}^{H+}}{\mathrm{DPE}} + f_{cov}^{TS} \frac{E_{cov}^{H+}}{\mathrm{DPE}} \quad (24)$$

are composite fractions that reflect a sum of the individual fractions of the DPE recovered by ionic and covalent interactions of the TS cation with conjugate anion, described in terms of the DPE components (E_{ion}^{H+}, E_{cov}^{H+}; acid properties independent of reactants or reaction; Table 3) and their respective fractions recovered by the TS cation (f_{ion}^{TS}, f_{cov}^{TS}; TS properties that do not depend on acid identity or properties; Table 5). The monomer formation energies (ΔE^{mono}) and protonated dimers (ΔE^{dimer}) can be described using thermochemical cycles analogous to Schemes 2 and 4 and relations of the form of eq 23 to give

$$\Delta E^{mono} = (1 - f_r^{mono})\mathrm{DPE} + \Delta E_{prot}^{mono} \quad (25)$$

for monomers and

$$\Delta E^{dimer} = (1 - f_r^{dimer})\mathrm{DPE} + \Delta E_{prot}^{mono} \quad (26)$$

for dimers, where f_r^{mono} and f_r^{dimer} represent the composite fractions reflecting both ionic and covalent individual fractions of DPE recovered by interactions of monomer and dimer cations, respectively, with the conjugate anion, which can be obtained by replacing $f_{ion/cov}^{TS}$ in eq 24 with $f_{ion/cov}^{mono}$ and $f_{ion/cov}^{dimer}$, respectively.

These values of the composite DPE fractions (sum of the individual ionic and covalent fractions) recovered by each species (f_r; eq 24) were calculated for each combination of Brønsted acid and surface species using the ionic and covalent DPE components (Table 3) and their recovered fractions for each surface species and TS (Table 5). The values of f_r^{mono} are near unity (0.89 to 0.90 for different POM clusters) because monomer cations resemble protons. The values of f_r^{dimer} (0.28 to 0.30) and f_r^{TS} (0.25 to 0.28) are, however, much smaller than unity because the cationic species present as dimers or transition states are larger than protons, leading to weaker ionic and covalent stabilization

dx.doi.org/10.1021/ja506149c | J. Am. Chem. Soc. 2014, 136, 15229−15247

by the conjugate anions than for protons. The $(1 - f_r) \times$ DPE term reflects an effective DPE, arising from differences between the energy required to deprotonate acids and that recovered by interactions of organic cations with conjugate anions; its magnitude can be estimated by rigorously incorporating the different covalent and ionic character of O−H bonds in each class of acids (eqs 23, 25 and 26). The monomer, dimer, and TS formation energies can be described in terms of $(1 - f_r^{mono}) \times$ DPE, $(1 - f_r^{dimer}) \times$ DPE, and $(1 - f_r^{TS}) \times$ DPE, respectively, using a single trend line for all acids (Mo and W POM clusters, mineral acids). This trend line has a slope of unity and an intercept that corresponds to the protonation energies to form gaseous analogues of each intermediate and of the TS (Figure 11; ΔE_{prot} values in Table 5); these are molecular properties that do not depend on the identity of the acid catalyst or its conjugate anion.

Monomer, dimer, and TS formation energies each correlate with their respective $(1 - f_r) \times$ DPE values (eq 23−26; Figure 11); therefore, the activation energies (E_a^{mono}, E_a^{dimer}, corresponding to measured k_{mono}, k_{dimer}) correlate with the difference between such values for the TS and for the respective reference states for each rate constant on all acids (as shown in the Supporting Information, Figure S8)

$$E_a^{mono} = (f_r^{mono} - f_r^{TS})\text{DPE} + (\Delta E_{prot}^{TS} - \Delta E_{prot}^{mono}) \quad (27)$$

$$E_a^{dimer} = (f_r^{dimer} - f_r^{TS})\text{DPE} + (\Delta E_{prot}^{TS} - \Delta E_{prot}^{dimer}) \quad (28)$$

The $(f_r^{mono} - f_r^{TS}) \times$ DPE and $(f_r^{dimer} - f_r^{TS}) \times$ DPE values reflect differences between the energies required to remove monomer and dimer cations, respectively, from their conjugate anions and the energy recovered by the interaction of the TS cation with the same conjugate anion. The $(f_r^{dimer} - f_r^{TS}) \times$ DPE values for dimers (21 to 28 kJ mol^{-1} for POM clusters; Supporting Information, Figure S8) are much smaller than the $(f_r^{mono} - f_r^{TS}) \times$ DPE values for monomers (688 to 720 kJ mol^{-1} for POM clusters and mineral acids; Supporting Information, Figure S8) because dimers closely resemble the charged nature of the TS species, whereas monomers form neutral H-bonded species that have stronger proton−anion interactions than TS−anion interactions. The measured first-order CH_3OH dehydration rate constants (k_{mono}) on Mo-POM clusters lie well below the trends for W-POM clusters (Figure 4a) as a function of DPE; in contrast, k_{mono} values as a function of $(f_r^{mono} - f_r^{TS}) \times$ DPE can be described by a single trend line for the two types of clusters (Figure 12). These treatments and their mechanistic inferences rigorously resolve the apparent disparity in reactivity for a given DPE for W and Mo POM clusters, which reflects the larger covalent component of monomer−anion (and proton−anion) interactions on Mo-POM than W-POM clusters; such covalent components cannot be fully recovered at ion-pair transition states (or dimers), making them less stable, in a manner that is accurately captured by the relations between activation energies and recovered DPE fractions (eqs 27 and 28).

Equations 23−26 and their conceptual basis provide a general and rigorous theoretical framework to describe molecular reactivity in acid catalysis; its application and the resulting conclusions are not restricted to any one class of Brønsted acids. These relations predict the formation energies of relevant surface species, and thus reactivity, for CH_3OH dehydration on Brønsted acids beyond those considered here when their ionic and covalent DPE components can be estimated from theory. They can also describe the energies of kinetically relevant species for reactions other than CH_3OH dehydration when the gas-phase

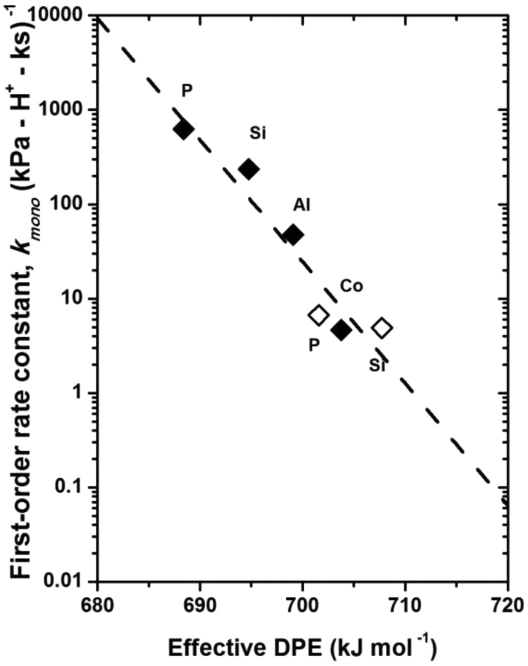

Figure 12. Measured k_{mono} values as a function of effective DPE values that reflect the net energy to remove a monomer-covered proton from POM clusters after subtracting the compensating interaction energy of TS cation with the conjugate anion, calculated as $(f_r^{mono} - f_r^{TS}) \times$ DPE (eq 27; f_r^{TS} and f_r^{mono} reflect fractions of the DPE of bare cluster recovered by TS−anion and monomer−anion interactions, respectively) on $H_{8-n}X^{n+}W_{12}O_{40}$ (closed diamonds) and $H_{8-n}X^{n+}Mo_{12}O_{40}$ (open diamonds) clusters ($X^{n+} = P^{5+}$, Si^{4+}, Al^{3+}, Co^{2+}). The dashed line reflects the best exponential regression fit to k_{mono} values.

protonation energies and the fractions of DPE components recovered by the gaseous analogues of such species, which do not depend on acid strength or identity, can be estimated from theory.

The approach described in this study shows that acids with more covalent (and less ionic) H−Z bonds but similar acid strength (and DPE) form less stable charged intermediates and transition states, leading to higher activation barriers for kinetic steps that reflect the stability of ion-pair transition states relative to neutral species. Covalent components of DPE depend on the effectiveness of charge delocalization in conjugate anions and therefore on their polarizability.[37,38] Smaller anions are less polarizable than larger anions ($E_{cov,mineral\ acid}^{H+} < E_{cov,POM}^{H^+}$; Figure 8); among large anions, those with larger HOMO−LUMO energy gaps tend to be less easily polarized[39] ($E_{cov,W\text{-}POM}^{H^+} < E_{cov,Mo\text{-}POM}^{H^+}$; Figure 8). Such trends lead us to expect that aluminosilicate acids, and specifically those with crystalline microporous structures (zeolites), would exhibit a smaller covalent component in their DPE than POM clusters because of their more insulating (and less polarizable) nature.[39] The less covalent nature of O−H bonds in zeolites may contribute to their higher reactivity than that predicted from DPE trends derived from rate constants on W-POM clusters,[12] which have been solely attributed to solvation via van der Waals interactions within voids of molecular dimensions.[12]

4. CONCLUSIONS

CH_3OH dehydration rate constants on Mo-POM clusters were compared with previously measured values on W-POM clusters[11] as a function of their calculated DPE values. The

dx.doi.org/10.1021/ja506149c | J. Am. Chem. Soc. 2014, 136, 15229−15247

stabilities of reactive intermediates and transition states on these two types of Keggin POM clusters and on gaseous mineral acids (H_2SO_4 and H_3PO_4) were also examined for comparison using theoretical methods. For a given DPE value, Mo-POM clusters show smaller first-order rate constants (Figure 4) and less stable intermediates and transition states than those for W-POM clusters (Figures 5 and 6), whereas such species are more stable on mineral acids than that expected from the stability−DPE trends observed on W-POM clusters (Figures 5 and 6). Our analysis shows that the less stable nature of TS and charged intermediates on Mo-POM clusters reflects a larger covalent component in their proton−anion interactions than on W-POM clusters (Figure 8). Such covalency is disrupted upon deprotonation but is not recovered fully upon forming the ion pairs at the transition states (Figure 10). These conclusions were rigorously reached using thermochemical cycles (Schemes 2 and 4) that describe the stability of surface species in terms of the interaction of protons and organic cations with conjugate anions and by dissecting these interactions into their respective covalent and ionic components. Similarly, surface species are more stable on mineral acids because their DPE values reflect a stronger ionic component than POM clusters. In this study, we have developed and described methods to calculate ionic and covalent components of DPE and other ion-pair interactions and a general framework to incorporate them into the descriptors of reactivity of solid acids (eqs 23−26). In doing so, we have illustrated how acid strength, described by the energy required to separate a proton (H^+) from the conjugate anion (Z^-) by cleaving an H−Z bond with a certain ionic character, influences the stability of an ion-pair transition state (TS^+-Z^-) with different ionic character than that of the corresponding H−Z bond in the acid.

■ ASSOCIATED CONTENT

Supporting Information

Primary and secondary reactions of CH_3OH-O_2 mixtures; calculation of electrostatic interaction energy between ion pairs; comparison of sequential and direct routes for methanol dehydration; derivation of DME formation rate expression; optimized bond distances and Bader charges of intermediates and transition states; effect of saturation of acid sites of POM cluster on DPE; structures of intermediates and transition states on POM clusters and H_2SO_4; charge density difference between neutral and anion POM cluster; thermochemical cycles to describe monomer and dimer formation energies; activation energies as a function of effective DPE; effects of DFT methods and parameters on the calculation results; and absolute energies and coordinates of optimized structures. This material is available free of charge via the Internet at http://pubs.acs.org.

■ AUTHOR INFORMATION

Corresponding Author

iglesia@berkeley.edu

Notes

The authors declare no competing financial interest.

■ ACKNOWLEDGMENTS

This material is based on work supported by the U.S. Department of Energy, Office of Science, Office of Basic Energy Sciences, under contract no. DE-AC05-76RL01830. Computational facilities were provided by the Environmental Molecular Science Laboratory (EMSL) at Pacific Northwest National Laboratory (PNNL), a DOE Office of Science User Facility, under proposal no. 47582. The use of molecular DFT calculations using Gaussian program was made possible by the Extreme Science and Engineering Discovery Environment (XSEDE) and a UC Berkeley College of Chemistry facility, which are supported by the National Science Foundation (grant nos. ACI-1053575 and CHE-0840505, respectively).

■ REFERENCES

(1) Macht, J.; Carr, R. T.; Iglesia, E. *J. Catal.* **2009**, *264*, 54−66.
(2) Pope, M. T.; Muller, A. *Angew. Chem., Int. Ed. Engl.* **1991**, *30*, 34−48.
(3) Okuhara, T.; Mizuno, N.; Misono, M. *Adv. Catal.* **1996**, *41*, 113−252.
(4) Misono, M. *Chem. Commun.* **2001**, 1141−1152.
(5) Macht, J.; Janik, M. J.; Neurock, M.; Iglesia, E. *Angew. Chem., Int. Ed.* **2007**, *119*, 8010−8014.
(6) Macht, J.; Carr, R. C.; Iglesia, E. *J. Am. Chem. Soc.* **2009**, *131*, 6554−6565.
(7) Knaeble, W.; Carr, R. T.; Iglesia, E. *J. Catal.* **2014**, *319*, 283−296.
(8) Brändle, M.; Sauer, J. *J. Am. Chem. Soc.* **1998**, *120*, 1556−1570.
(9) van Santen, R. A.; Kramer, G. J. *Chem. Rev.* **1995**, *95*, 637−660.
(10) Macht, J.; Janik, M. J.; Neurock, M.; Iglesia, E. *J. Am. Chem. Soc.* **2008**, *130*, 10369−10379.
(11) Carr, R. C.; Neurock, M.; Iglesia, E. *J. Catal.* **2011**, *278*, 78−93.
(12) Jones, A. J.; Carr, R. C.; Zones, S. I.; Iglesia, E. *J. Catal.* **2014**, *312*, 58−68.
(13) Janik, M. J.; Macht, J.; Neurock, M.; Iglesia, E. *J. Phys. Chem. C* **2009**, *113*, 1872−1885.
(14) Argyle, M. D.; Chen, K.; Resini, C.; Krebs, C.; Bell, A. T.; Iglesia, E. *J. Phys. Chem. B* **2004**, *108*, 2345−2353.
(15) Deshlahra, P.; Carr, R. C.; Chai, S.; Iglesia, E., submitted to *ACS Catal.*
(16) (a) Kresse, G.; Hafner, J. *Phys. Rev. B* **1993**, *47*, 558−561. (b) Kresse, G.; Furthmuller, J. *Comput. Mater. Sci.* **1996**, *6*, 15−50. (c) Kresse, G.; Furthmuller, J. *Phys. Rev. B* **1996**, *54*, 11169−11186.
(17) Vanderbilt, D. *Phys. Rev. B* **1990**, *41*, 7892−7895.
(18) Perdew, J. P.; Chevary, J. A.; Vosko, S. H.; Jackson, K. A.; Pederson, M. R.; Singh, D. J.; Fiolhais, C. *Phys. Rev. B* **1992**, *46*, 6671−6687.
(19) Makov, G.; Payne, M. C. *Phys. Rev. B* **1995**, *51*, 4014−4022.
(20) Jónsson, H.; Mills, G.; Jacobsen, K. W. *Classical and Quantum Dynamics in Condensed Phase Simulations*; Berne, B. J., Coccotti, G., Coker, D. F., Eds.; Kluwer Academic: New York, 1998; p 385.
(21) Henkelman, G.; Jónsson, H. *J. Chem. Phys.* **1999**, *111*, 7010−7022.
(22) Kresse, G.; Joubert, D. *Phys. Rev. B* **1999**, *59*, 1758−1775.
(23) Frisch, M. J. et al. *Gaussian 09*; Gaussian, Inc.: Wallingford CT, 2009.
(24) Feynmann, R. P. *Phys. Rev.* **1939**, *56*, 340−343.
(25) Ma, Y.; Politzer, P. *J. Chem. Phys.* **2004**, *120*, 8955−8959.
(26) Gavezzotti, A. *J. Phys. Chem. B* **2002**, *106*, 4145−4154.
(27) Volkov, A.; Coppens, P. *J. Comput. Chem.* **2004**, *25*, 922−934.
(28) Bader, R. *Atoms in Molecules: A Quantum Theory*; Oxford University Press: New York, 1990.
(29) (a) Henkelman, G.; Arnaldsson, A.; Jónsson, H. *Comput. Mater. Sci.* **2006**, *36*, 354−360. (b) Sanville, E.; Kenny, S. D.; Smith, R.; Henkelman, G. *J. Comput. Chem.* **2007**, *28*, 899−908.
(30) (a) King-Smith, R. D.; Vanderbilt, D. *Phys. Rev. B* **1993**, *47*, 1651−1654. (b) Politzer, P.; Stout, E. W. *Chem. Phys. Lett.* **1973**, *8*, 519−522.
(31) Baertsch, C. D.; Komala, K. T.; Chua, Y.-H.; Iglesia, E. *J. Catal.* **2002**, *205*, 44−57.
(32) Janik, M. J.; Bardin, B. B.; Davis, R. J.; Neurock, M. *J. Phys. Chem. B* **2006**, *110*, 4170−4178.
(33) Kazansky, V. B. *Acc. Chem. Res.* **1991**, *24*, 379−383.
(34) (a) Soares, A. P. V.; Portela, M. F.; Kiennemann, A. *Catal. Rev.* **2005**, *47*, 125−174. (b) Mars, P.; van Krevelen, D. W. *Chem. Eng. Sci.* **1954**, *3*, 41−59.

(35) Aronson, M. T.; Gorte, R. J.; Farneth, W. E. *J. Catal.* **1986**, *98*, 434−443.
(36) Yang, S. C.; Stwalley, W. C. *ACS Symp. Ser.* **1982**, *179*, 241−254.
(37) Fajans, K. *Naturwissenschaften* **1923**, *11*, 165−172.
(38) French, S. J. *J. Chem. Educ.* **1936**, *1*, 122−130.
(39) Dimitrov, V.; Sakka, S. *J. Appl. Phys.* **1996**, *79*, 1736−1740.